Showcasing research from PD Dr. Majd Al-Naji's laboratory, BasCat – UniCat BASF JointLab of Technische Universität Berlin, and Institute of Chemical Technology at Universität Leipzig, Germany.

Electrocatalytic valorization of lignin

This tutorial review provides a deep knowledge on the current state of lignin valorization *via* electrocatalytic oxidation and/or reduction, as well as the recent challenges and future perspectives in electrocatalytic valorization of lignocellulosic biomass.

Image reproduced by permission of Majd Al-Naji from *RSC Sustainability*, 2026, **4**, 2042.

As featured in:

See Majd Al-Naji *et al.*,
RSC Sustainability, 2026, **4**, 2042.

ROYAL SOCIETY
OF **CHEMISTRY**

rsc.li/rscsus

Check for updates

Electrocatalytic valorization of lignin

Muhammad Bilal, [a] Prashanth W. Menezes, [b] Arne Thomas, [c] Reinhard Schomäcker, [d] Matthias Drieß, [e] Frank Rosowski[af] and Majd Al-Naji [*ag]

Lignin is the largest resource of biobased renewable aromatic feedstock for chemicals and fuels. For profitable biorefineries, lignin valorization is essential, as it enhances the overall efficiency of biomass conversion and improves process economics. In recent decades, lignin valorization and depolymerization processes have attracted significant scientific interest. Many approaches have been explored, including thermochemical methods, such as pyrolysis, oxidative depolymerization, and reductive catalytic fractionation; biological methods, like enzymatic depolymerization and microbial degradation; and electrochemical techniques, such as electrocatalytic oxidation and electrocatalytic hydrogenation. Among them, electrochemical processes play a significant role in lignin valorization by employing green electricity sources with *in situ* hydrogen generation, being environmentally friendly, and contributing to the economic feasibility of lignin conversion. In this review, the electrochemical conversion of lignin from lignocellulosic biomass, including lignin fractionation or depolymerization to lignin derived compounds (such as vanillin, benzoic acid and quinones) through electrocatalytic oxidation, and its upgrading through electrocatalytic hydrogenation or hydrogenolysis to produce industrially valuable lignin-based chemicals, are discussed in detail. Finally, a summary of current challenges, limitations and emerging opportunities in electrochemical valorization of lignin is provided to frame this technology for sustainable and biobased development.

Sustainability spotlight

Electrocatalytic lignin valorization enables the production of bio-based products by mitigating the environmental impact of fossil-based industries. Transforming lignin into valuable products is guided by the 12 principles of green chemistry. This approach lies within the UN Sustainable Development Goals, SDG 7 (Affordable and Clean Energy) and SDG 12 (Responsible Consumption and Production). This approach produces industrially relevant chemicals by replacing the overdependence on fossil-based resources, thereby lowering greenhouse gas emissions, thus contributing to SDG 9 (Industry, Innovation, and Infrastructure) and SDG 13 (Climate Action). This review proposes a green electrochemical approach to valorize lignin through oxidation or reduction processes, aiming to produce value-added green products that have high sustainability metrics, advancing the transition towards a more sustainable and circular economy.

1. Introduction

The continuous growth of the population has resulted in steadily increasing consumption of fossil resources, leading to the environmental problems of today.[1] However, biomass, solar energy, wind, and hydrogen produced *via* water electrolysis are considered renewable and sustainable resources with zero carbon emissions.[2] Among them, lignocellulose biomass (LCB) has been widely investigated as a viable raw material and alternative to fossil-based resources for the generation of bi-ofuels, fine chemicals, and bioproducts.[3–5] With an estimated 550 Gt of biomass, LCB is the largest organic matter reservoir on Earth.[6] LCB is an important resource from the plant cell wall, typically composed of carbohydrates with cellulose making up 40–50%, hemicellulose making up 15–30% of biomass, and non-carbohydrate streams like lignin accounting for 15–30%, which is polyaromatic.[7,8] Cellulose is a homopolymer that contains repeating units comprised of a disaccharide in which glucose units are linked through a β-1,4-glycosidic linkages in its chain, while hemicellulose, a heteropolymer, is mainly composed of condensed monosaccharides, C5 and C6 units

ᵃBasCat-UniCat BASF JointLab, Technische Universität Berlin, Hardenbergstrße 36, Sekr. EW K-01, 10623 Berlin, Germany. E-mail: majd.al-naji@tu-berlin.de

ᵇDepartment of Materials Chemistry for Catalysis, Helmholtz-Zentrum Berlin für Materialien und Energie, 12489 Berlin, Germany

ᶜDepartment of Chemistry, Functional Materials, Technische Universität Berlin, 10623 Berlin, Germany

ᵈInstitute of Chemistry-Technical Chemistry, Technische Universitat Berlin, Berlin, Germany

ᵉDepartment of Chemistry, Metalorganics and Inorganic Materials, Technische Universität Berlin, Straße des 17. Juni 115, Sekr. C2, 10623 Berlin, Germany

ᶠBASF SE, Carl-Bosch-Straße 38, 67056 Ludwigshafen, Germany

ᵍInstitute of Chemical Technology, Universität Leipzig. Linnéstraße 3, 04103 Leipzig, Germany. E-mail: majd.al-naji@uni-leipzig.de

(Fig. 1).[9–16] Hemi(cellulose) and lignin together provide structural integrity to plant cell walls. Both cellulose and hemicellulose have been extensively investigated for the production of sugars and sugar derivatives such as furfural alcohol, hydroxymethylfurfural (HMF), and organic acids.[17,18] However, lignin is considered an underutilized material, often burnt for energy or recovered as part of chemical recovery from the pulping process.

Lignin is a three-dimensional, heterogeneous aromatic polymer primarily composed of phenolic alcohols. Due to its chemical composition, lignin is a major source of aromatic chemicals from bio-based feedstock.[19] When compared to cellulose and hemicellulose, which have higher O contents of 30 and 49%, lignin exhibits a higher heating value of 40% due to a higher H/C ratio.[20–22] Moreover, lignin acts as a cellular glue by providing plant tissues and fibres with compressive strength and showing resistance to disease and insects. Lignin's structure is mainly composed of three different monolignols, including *p*-coumaryl alcohol, coniferyl alcohol, and sinapyl alcohol, which correspond to *P*-hydroxylphenol (H), guaiacyl (G), and syringyl (S) units in the lignin matrix (Fig. 1).[21,23–26] These monolignols form diverse inter-unit connections of C–C or ether bonds. The most frequent lignin connections currently understood are 50–80% ether bonds (β-O-4, α-O-4, spiro-dienone (β-1), phenyl coumaran (β-5), resinol (β–β), diphenyl ether (4-O-5), and biphenyl (5–5′), although research to discover new linkages is still underway.[23,25,27,28] Among these various linkages, the β-O-4 ether linkage is the predominant and least stable linkage, making it easy to cleave. Due to this reason, these ether linkages in lignin have received great attention.[25,27] In comparison to cellulose, lignin lacks the regular repeating pattern of monolignols.[21,29,30] In the context of plant taxonomy,

Muhammad Bilal received his bachelor's degree in chemistry from the University of Wah, Pakistan. Then he finished his master's thesis on water splitting at Quaid-i-azam University, Pakistan. Currently, he is pursuing his PhD at the Technical University Berlin, where his research focuses on converting renewable sources (lignocellulosic biomass) into drop-in chemicals funded by the Cluster of Excellence Unifying Concept in Catalysis (UniSysCat). His research interests include heterogeneous catalysis and electrocatalysis for water splitting & biomass conversion.

Muhammad Bilal

Dr Prashanth W. Menezes is the head of the Department of Materials Chemistry for Catalysis at Helmholtz-Zentrum Berlin. He received his PhD from the Max Planck Institute for Chemical Physics of Solids in Dresden, following which he moved to Technische Universität München and then to Technische Universität Berlin to work on energy catalysis. His research focuses on the design, development, and dynamic understanding of unconventional catalysts in heterogeneous catalysis, especially in the area of redox oxygen catalysis and (photo)electrocatalytic water splitting, CO_2 reduction and electrochemical redox waste valorisation reactions.

Prashanth W. Menezes

Arne Thomas is a full professor of functional materials at the Department of Chemistry of Technische Universität Berlin. He received his PhD from the Max Planck Institute of Colloids and Interfaces in Potsdam, Germany. After a postdoctoral stay at the University of California, Santa Barbara, as an AvH fellow, he rejoined the MPIKGF as a group leader. In 2009, he became a professor at Technische Universität Berlin, where he leads the Department of Functional Materials. His research focuses on porous materials—from mesoporous inorganic to microporous organic materials.

Arne Thomas

Reinhard Schomacker received his Diploma and his Doctoral Degree in Physical Chemistry at the University of Bielefeld. In 1987 he joined the group of Professor M. Kahlweit at the Max-Planck-Institute for Biophysical Chemistry in Gottingen for studies on the thermodynamics and structures of microemulsions and lyotropic liquid crystals. Then, he joined the chemical engineering group of the Central Research Laboratories of Bayer AG in Leverkusen. In 1992 he completed his Habilitation in physical chemistry with Professor D. Woermann at the University of Cologne. Since 1996, he has been a full professor in Chemical Engineering at the Department of Chemistry at TU Berlin.

Reinhard Schomäcker

the arrangement of H, G, and S monolignols varies, resulting in different forms of biomass. In general, hardwood lignin (angiosperm) is primarily composed of G and S units in varying ratios, softwood lignin (gymnosperm) is almost entirely made up of G units, compression wood is mainly composed of H and G units, while all the H, G, and S units are present in grass lignin (Fig. 2).[31–34]

According to reports,[3,35] over 50 million tonnes of waste lignin are produced annually from the pulping sector. Unfortunately, out of this, merely 5% of waste lignin is utilized for large-scale applications such as the generation of electricity and heat, with the majority being burned or abandoned.[36] Undoubtedly, it is the third most abundant component of LCB, but its utilization is very low, which results in major resource loss and high disposal costs.[37] In summary, lignin valorization not only produces bio-based products by utilizing waste but also eliminates the excessive use of fossil fuels to overcome the energy crisis and contributes to global environmental protection.[38]
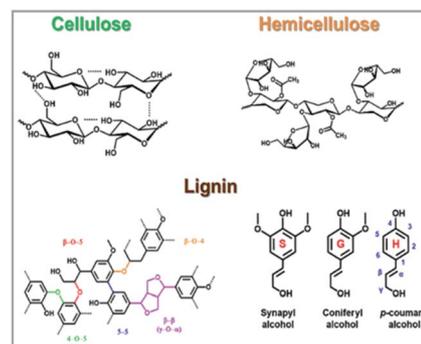

Fig. 1 Three primary components of LCB and lignin monolignols. Reproduced from ref. 6 *Chem. Ing. Tech.*, 2022, **94**, 1611–1627, under a CC-BY license.

Typically, industrially relevant lignin produced from the paper and pulp industry and other biorefineries is referred to as "technical lignin". The main sources of technical lignin are kraft lignin (KL) (obtained by treating biomass with NaOH and sodium sulfide at 170 °C by cleaving the bonds between lignin and cellulose), organosolv lignin (OL) (produced by processing biomass with an ethanol/water mixture at 200 °C at 20–30 bar for a few hours to separate the lignin from the carbohydrate stream), soda lignin (SL) (13–16% alkali is used to delignify the non-woody biomass at 140–170 °C), and lignosulfonate (LS) (obtained by treating LCB with sulfurous acid and sulfite salt at various pH values; this process involves two reactions, *i.e.*, hydrolysis and sulfonation). The structure of different types of technical lignin is shown in Fig. 3.[39] All of these lignins are water insoluble except LS, which is highly soluble. The lignin obtained from these processes are complex heterogeneous polymers with high molecular weight and condensed structures. Moreover, the structure and functionality of technical lignin are different from those of native lignin, except for organosolv lignin, which shows close resemblance due to its sulfur-free structure but is still modified. This structural complexity and impurities in technical lignin lower its potential

Matthias Drieß is a Full Professor of metalorganics and inorganic materials at TU Berlin since 2005. He obtained his PhD degree and completed his habilitation at the University of Heidelberg. He served as a Full Professor of Inorganic Chemistry at Ruhr Universität Bochum (1996–2004). He served as a spokesperson for the Clusters of Excellence UniCat, and UniSysCat. He is one of the scientific directors of BasCat – UniCat BASF JointLab at TU Berlin and a director of the Chemical Invention Factory (CIF). He is a member of the German National Academy of Sciences (Leopoldina), Berlin-Brandenburg Academy of Sciences and Humanities, and European Academy of Sciences.

Matthias Drieß

Frank Rosowski is a scientific director of BasCat – UniCat BASF JointLab Technische Universität Berlin since 2012. He studied Chemistry at Technische Universität Berlin. Then, he completed his PhD under the supervision of the Nobel laureate Prof. Dr Gerhard Ertl at the Fritz Haber Institute of the Max Planck Society. In 1996, he joined BASF SE and has worked in a wide range of heterogeneously catalyzed chemical reactions.

Frank Rosowski

PD Dr Majd Al-Naji obtained his MSc (2013) and PhD (2017) from Universität Leipzig. He subsequently completed his habilitation and received the "Privatedozent" title in 2024 from Universität Leipzig. He was a postdoctoral researcher at KU Leuven with Prof. Dr Bert F. Sels. He led the "Biorefinery and Sustainable Chemistry" group at the Max Planck Institute of Colloids and Interfaces (2018–2021). From 2023 to 2025, he was a group leader of the Sustainable Value Chains group at the BasCat – UniCat BASF JointLab at TU Berlin. He is currently serving as an interim professor at the Institute of Chemical Technology, Universität Leipzig.

Majd Al-Naji

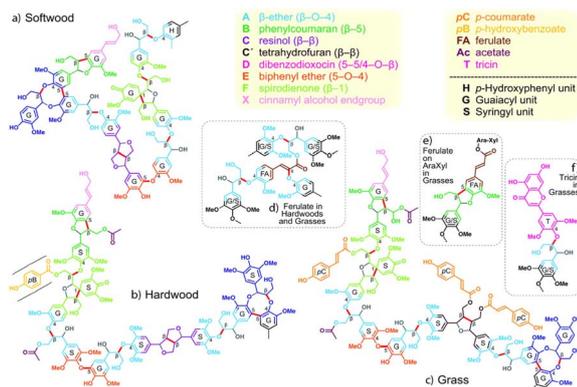© 2026 The Author(s). Published by the Royal Society of Chemistry

Fig. 2 Three different types of lignin structures found in softwood (a), hardwood (b), and grass (c). The predominant and frequently occurring lignin connections are indicated using their corresponding colours. Adapted from ref. 3 *Energy Environ. Sci.*, 2021, **14**, 262–292, under the terms of a CCA 3.0 license.

for high-value products; rather, it is utilized as a low-value fuel.[40]

Therefore, various approaches have been employed to convert lignin into value-added chemicals, such as acid/base catalysis, (hydro)thermal treatment, reductive catalytic fractionation (RCF), and oxidative catalytic fractionation (OCF).[41] However, there are several potential obstacles that must be addressed. Thermal depolymerization typically requires high temperatures (200–400 °C) and elevated hydrogen pressures (100–200 bar), which pose significant challenges for upgrading bio-oils with high oxygen content.[42,43] OCF, on the other hand, can proceed under relatively mild conditions (30–250 °C) to form several functional chemicals such as aromatic aldehydes, alcohols, and acids.[41] Nevertheless, the presence of uncontrolled radical intermediates often leads to recondensation to form new C–C single bonds, ultimately reducing product

Fig. 3 Representation of the simplified structure of technical lignin. Adapted from ref. 40 *Int. J. Mol. Sci.*, 2020, **22**, 63, under the terms of the CC-BY license.

selectivity. The RCF of LCB forms a solid pulp (carbohydrate) and lignin oil through cleavage of ether and ester bonds *via* simultaneous high temperature and H_2 pressure, utilizing either batch or semi-continuous modes of the reactor.[44] It is generally accepted that the formation of unreactive condensed lignin derivatives is prevented by stabilizing the reactive intermediates produced by the depolymerization of plant lignin.[25] This approach completely delignified hardwoods like poplar and birch without significant degradation of their carbohydrates. In addition to low-molecular-weight oligomers, lignin oil has a small number of phenolic monomer yields that are nearly theoretical maximum, specifically upto ~50% for hardwoods.[33] However, the requirement for high hydrogen pressure remains a significant drawback. These methods are excellent for lignin depolymerization, but each has its own limitations that must be overcome in order to achieve commercial application of lignin valorization.

In this regard, electrochemical methods are considered to be environment-friendly, reagent-free, and cost-effective approaches for lignin conversion; moreover, these approaches can be performed under moderate reaction conditions.[45–50] Electrochemical oxidation and reduction are processes where chemical species undergo oxidation (loss of electrons) and reduction (gain of electrons) at the anode and cathode, respectively. In electrochemical oxidation, the organic species or lignin is oxidized at the anode and favors the formation of value-added oxygenated products like aldehydes, ketones, and carboxylic acids, while at the cathode, the reduction promotes hydrogenated products like hydrocarbons and alcohols depending upon the feedstock, electrolyte, and catalyst employed. The dominant competing side reactions in aqueous media are the oxygen evolution reaction (OER) and hydrogen evolution reaction (HER) at the anode and cathode, respectively. These electroorganic reactions have gained significant interest; they utilize renewable energy for the formation of drop-in chemicals and prevent the use of harsh chemicals like oxidizing and reducing agents. The electrocatalytic valorization of lignin yields a wide range of targeted products, which can be classified based on their applications. Lignin-derived aromatic monomers, including vanillin, guaiacol, and syringaldehyde, have high market potential and are used as valuable precursors for the synthesis of fine chemicals, flavors, and pharmaceuticals.[46] The phenolic compounds such as phenol, cresols, and catechol serve as precursors for polymers, resins, and adhesives.[51] The oxidation products of lignin, such as dicarboxylic acid (adipic acid and muconic acid, *etc.*) and quinones (benzoquinone and anthraquinone derivatives), are promising candidates for biopolymer synthesis and redox flow batteries, while reductive strategies form alkanes and cycloalkanes that are used as biofuels.[52,53] In these product-based classifications, the aromatic monomers and phenolic compounds have high selectivity in electrocatalytic processes and strong market relevance, making them a favorable bio-based substitute for traditional fossil-derived chemicals. Therefore, future research should prioritize strategies to specifically target these classes, along with the development of redox-flow molecules for energy applications.
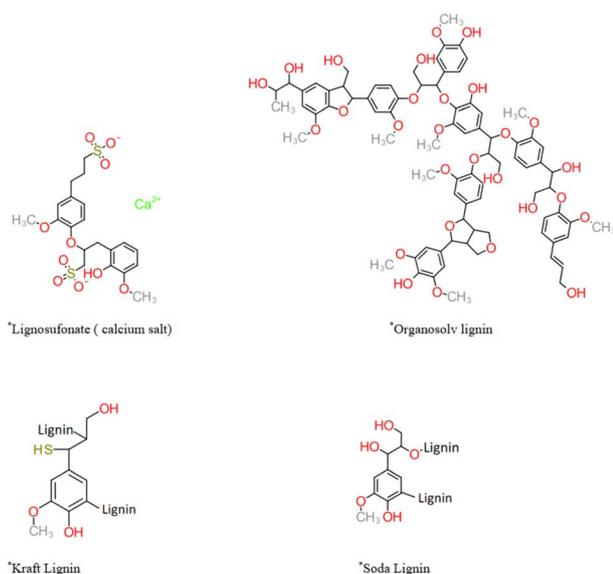
To assess the performance of electrochemical conversions, it is essential to understand the product identification and quantification techniques. To identify the products, gas chromatography with mass spectrometry (GC-MS for volatile compounds), high-performance liquid chromatography with mass spectrometry (HPLC-MS for polar compounds), and 1D and 2D nuclear magnetic resonance (NMR) are commonly used techniques for structural elucidation, while gas chromatography with flame ionization detection (GC-FID), HPLC, and NMR are also used for quantification purposes. The following key parameters help determine the reaction metrics for lignin model compounds:

$$\text{Current density} = \frac{\text{current (mA)}}{\text{geometric area of working electrode (cm}^2)}$$

Conversion:

The amount of reactant transformed into chemical products is expressed as:

$$\text{Conversion (\%)} = \frac{\text{initial moles} - \text{moles left}}{\text{initial moles of reactant}} \times 100$$

Selectivity:

$$\text{Selectivity (\%)} = \frac{\text{moles of targeted product}}{\text{total moles of products}} \times 100$$

Yield:

$$\text{Yield (\%)} = \text{conversion} \times \text{selectivity} \times 100$$

Faradaic efficiency:

$$\text{Faradaic efficiency (\%)} = \frac{\text{moles of product} \times n \times F}{Q_{\text{total}}} \times 100$$

n = electrons required to form a particular product, F = Faraday's constant (96 485C), and Q_{total} = total charge passed.

1.1. Key electrochemical performance metrics for real lignin

In contrast to small lignin-derived aromatics or model compound electrocatalysis, electro-valorization of real lignin involves a complex heterogeneous polymeric substrate with ambiguous molecular weight and composition. Therefore, traditional electrochemical performance metrics such as conversion, selectivity, yield, and FE need distinct interpretation compared to single-compound reactions.

1.1.1. Conversion. The conversion of lignin cannot be defined based on the moles of reactant used, as in the case of simple lignin-derived compounds. Instead, it is quantified as mass loss of insoluble lignin, the reduction in molecular weight determined by GPC, or the bond cleavage of certain linkages such as β-O-4 and β–β, measured by 2D-HSQC NMR.[54] These methodologies are collectively needed to describe the depolymerization of lignin due to its complex nature.

1.1.2. Selectivity and yield. Selectivity is calculated based on a specific product (*e.g.*, phenol, syringaldehyde, vanillin, and benzoic acid) relative to the total products identified in the soluble fractions, while the yield of lignin products is determined with respect to carbon content, or the mass of monomeric or oligomeric products identified *via* GC-MS, HPLC, or LC-MS, relative to the starting lignin mass.[55,56] The oligomeric products are quantified through mass balance with solvent-extracted fractions or by integrating the peaks obtained from chromatography.

1.1.3. Faradaic efficiency. FE is defined based on a particular reaction pathway or product rather than the lignin polymer as a whole. The calculation involves assigning electron stoichiometry to a particular conversion, such as alcohol to aldehyde, which requires two electrons, and further oxidation of aldehyde to acid, which needs two more electrons, and then correlating the quantity of product produced to the total charge transferred. In the case of bond-breaking reactions, which are promoted by radical pathways, which is itself a chemical process, FE is calculated based on the formation of the product instead of the cleavage of a particular bond.[57] Different reports use distinct analytical methodologies and principles; however, it's still challenging to compare absolute FE and yield.[57] Nonetheless, comparative data within a specific experimental context provide significant insights for catalyst and reactor design.

Electrocatalytic methods have gained a significant dominance in scientific community due to their inherent advantages. Therefore, both cellulose and hemicellulose are widely investigated *via* electrocatalysis and are therefore not discussed in this article. In contrast, for lignin, many review articles have been reported with a focus on lignin extraction from wood or have separately discussed electrocatalytic oxidation and reduction of lignin monomers/model compounds and technical lignin.[46,58–61] Specifically, Liu *et al.*[62] reported a comprehensive overview of reaction types and catalyst categories. In comparison, this review article explicitly provides the process and mechanistic insights, treating both EO and ECH as complementary processes within the framework of lignin valorization. Instead focusing only of reaction types, this review highlights (i) how electrocatalysis modifies the depolymerization of lignin by employing renewable energy compared to conventional thermochemical processes, (ii) how metal–support interaction, electrolyte composition, current density, reactor design, and membrane technologies control the selectivity and FE, and (iii) how both EO and ECH processes can be integrated to suppress the repolymerization and overoxidation of the products. Electrode-level design and reaction key metrics were particularly emphasized to distill actionable design rules for the new researcher entering the field.

2. Electrochemical oxidation (EO) of lignin

The lignin depolymerization *via* EO is conducted under ambient conditions and represents an environmentally sustainable and promising method. In this approach, lignin or

its model compounds are oxidized at the anode *via* an electron transfer process which involves the oxidation of aromatic alcohol and lignin side chains to various products, including aldehydes, ketones, and carboxylic acid, while cleavage of β-O-4 or other ether linkages is performed *via* radical-driven and electro-assisted solvolytic processes. Moreover, the over-oxidation of products can be avoided by tuning the applied voltage, which allows better control over selectivity. The depolymerization process occurs under mild conditions, eliminating the requirement for high temperature and pressure.

2.1. Electrochemical oxidation pathways of lignin conversion

EO is the most commonly used method for electrochemical lignin conversion to various products. The actual anodic oxidation of lignin yields oxygenated products such as syringaldehyde, vanillin, 3,4-dimethoxybenzaldehyde, benzoic acid, *etc.*[63] While non-oxidized products such as 1,2-dimethoxybenzene and resinol are formed by the coupling of side chains or bond cleavage driven by the radical mediator. To convert technical lignin and lignin model compounds, primarily three electro-oxidation approaches have been studied, including direct oxidation, indirect oxidation, and electrical–chemical combination reactions, which also involve indirect oxidation by small molecules (Fig. 4).[58]

The EO of lignin does not proceed *via* a single reaction pathway. However, depending upon the applied potential, electrode material, and electrolyte composition, three different mechanistic pathways are operated in parallel: (i) The direct EO of lignin often utilizes a heterogeneous catalyst (*e.g.*, Ni, Co, Cu, SnO_2, RuO_2, or PbO_2), which can be either deposited on the conductive substrate or employed directly as the electrode itself.[64–68] On the anode surface, water oxidation and the oxidation of benzylic alcohol or side chains take place simultaneously. However, for these electrochemical processes, the ability of lignin to dissolve, the stability of the electrolyte, and proton/electron conduction are major challenges because electrochemical methods are limited to surface catalysis. (ii) Homogenous redox mediators, such as polyoxometalates (POMs), *N*-hydroxyphthalimide (NHPI), or ferric chloride, are used as an oxidizing agent and an electron or proton reservoir for indirect EO of lignin.[63,69,70] Aldehydes, ketones, and carboxylic acids are produced by this indirect EO of benzylic alcohol or

side chains, promoted by these redox mediators before they are regenerated or oxidized on the anode surface. Regarding the reaction involving a homogeneous redox mediator at the anode, lignin is present in the form of a slurry in the electrolyte. (iii) In addition to direct and redox mediator pathways, the depolymerization of lignin can be mediated by ROS species (*e.g.*, $^\bullet O_2^-$, $^\bullet OH$, and H_2O_2) produced electrochemically (*e.g.*, H_2O_2 and $^\bullet OH$ produced *via* the oxygen reduction reaction (ORR)), which involves the cleavage of C–O and C–C bonds *via* a radical-driven process that does not require a change in the oxidation state, resulting in the production of alcohols, phenols, and aromatic hydrocarbons. For lignin conversion, mainly two major competing reactions are the fission of C–O/C_α–C_β bonds (0.1–0.2 eV) and active functionalization of the hydroxyl group into the carbonyl group, *i.e.*, C_α-carbonylation. For lignin degradation, the cleavage of the β-O-4 linkage is a slow step reaction and determines the rate of reaction as it dominates in both hardwood (60%) and softwood (45–50%). Recent studies on lignin conversion suggest that oxidation *via* chemical methods, including the use of 2,2,6,6-tetramethyl-1-piperidinyloxy (TEMPO),[71] *N*-hydroxyphthalimide (NHPI),[72] 2,3-dichloro-5,6-dicyano-1,4-benzoquinone (DDQ),[73] and pyridium dichromate (PDC), is effective in oxidizing α-hydroxyl groups in β-O-4 ether linkages by improving both lignin degradation and yield.[74] However, EO is considered to be a viable alternative for the conversion of α-hydroxyl to α-carbonyl groups in lignin, or by reducing the use of hazardous and costly chemicals. To date, electrochemical methods have mainly focused on redox mediator assisted oxidation of benzylic alcohol and ROS mediated cleavage of C–C or C–O bonds in β-O-4 linkage to form lignin monomers.[75]

2.1.1. Direct electrochemical oxidation of lignin and counter-reaction on the cathode. Numerous direct EO studies have been reported in which lignin depolymerization by the electrochemical method effectively proceeds at the anode *via* the electron transfer process. At the same time, the applied anodic potential generates radicals and ROS, which are chemically involved in the cleavage of C–O and C–C bonds in the most common β-O-4 aryl ether linkage.[55] The most common cleavage in β-O-4 is of the C_α–C_β bonds. However, direct EO is a redox process which does not involve the scission of ether linkages; instead, this ether bond cleavage proceeds *via* electrochemically induced radicals or nucleophilic attack. Along with the depolymerization or functionalization of lignin, some side reactions, such as polymerization, also take place. Lignin monomers could be polymerized by two major processes, including intermolecular condensation or radical coupling reactions under less alkaline conditions and low temperatures.

By adding lignin to an aqueous basic solution (1 M NaOH) at the anode, the sluggish OER is replaced; the oxidation of lignin can occur along with the lowering of cell voltage that is required for the HER at the negative electrode.

Fig. 5 highlights the three mechanistic routes for EO of lignin and their possible product distribution.

For water oxidation the thermodynamic potential is 1.23 V, which is significantly higher than the minimum thermodynamic cell voltage (0.21 V) needed for lignin-assisted water
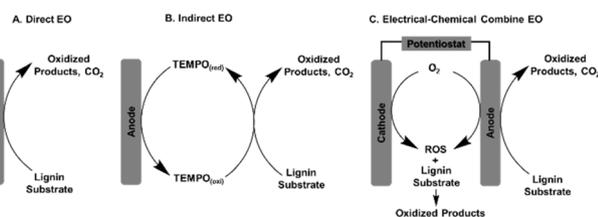

Fig. 4 Typical routes of lignin electrochemical oxidation (EO): (A) direct oxidation, (B) indirect oxidation, and (C) electrical–chemical combined oxidation. Reproduced from ref. **58** with permission from *ChemSusChem.*, 2020, **13**, 4318–4343. Copyright 2020, John Wiley and Sons.
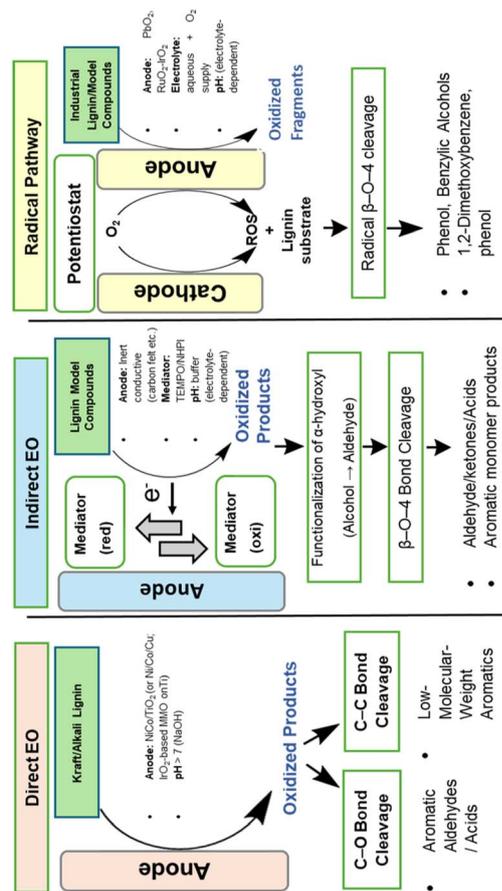
Fig. 5 Three mechanistic pathways (direct, indirect, and ROS-mediated radical pathways) of EO of lignin. The main reaction pathway primarily depends on the type of lignin used, the electrode material, and the electrolyte composition (pH).

electrolysis, highlighting that low energy is required for lignin oxidation compared to OER.[58] Furthermore, the low positive overpotential generates CO_2 and suppresses the formation of oxygen at the anode.[76] Both the lignin oxidation rate at the anode and the hydrogen evolution rate at the cathode can be enhanced by using $NiCo/TiO_2$ as an anodic electrocatalyst. This approach is considered cheaper as it reduces the cost of energy consumption in contrast to commercial alkaline water splitting, as both processes require lower overpotential than that needed for the OER.[77] The electrocatalyst β-PbO_2 on multi-walled carbon nanotubes also exhibited comparable effects, as reported by Bateni et al.[78] Overall, lignin depolymerization by EO produces low-molecular-weight fractions at the anode; this oxidation requires a lower anodic potential, thus reducing the total cell voltage by replacing OER with lignin oxidation.

2.1.1.1 Exploration of various anode types for lignin depolymerization. The lignin conversion rate and product selectivity are both significantly influenced by the anode catalysts, which are crucial for the efficient oxidation of lignin. For direct EO, the anodic electrode should be catalytically active for lignin depolymerization and stable toward anodic corrosion. Currently, reported electrodes include various transition metals (Ni, Co, and Cu), metal oxides (PbO_2, SnO_2, and IrO_2), and metal alloys

(alloys of Ti, Co, and Ni) that have been effectively used for lignin depolymerization.

2.1.1.1.1 Metal oxide/mixed metal oxide-based anode. Metal oxide (MOx)-based anodes have been extensively investigated for lignin depolymerization reactions due to their inherent electrocatalytic activities for organic oxidations.[66,79–81] The MOx surfaces provide potential inner-sphere electron-transfer routes that can enhance lignin oxidation compared to graphite electrodes. Early reported attempts in this field were made by Brooks et al.,[81] who showed EO in 1% NaOH solution of butanol-based Organosolv-lignin, employing oxidized lead as an anode.

Lead oxide is considered toxic but it is still frequently used as an electrode material for lignin EO because of its well-known chemical stability in acidic electrolytes, high overpotential for OER, excellent conductivity, and comparatively lower cost relative to noble metals. In comparison to raw lignosulfonate, electrocatalytically degraded lignosulfonate on the PbO_2 membrane electrode shows oil–water interfacial tension and reduced surface tension. After electrocatalytic degradation, numerous low molecular weight lignin fragments were formed, and along with these, due to condensation, large molecular weight lignin was also obtained. Voltage, current density, temperature, composition of electrolyte (pH), catalyst textural properties, and diffusivity of reactants and products are the main factors that control the conversion and product distribution.[67] Initially, the hydroxyl, phenolic, aldehyde, and carboxyl functionalities increase; however, with continuous electrolysis over time, their content significantly decreases without affecting the sulfonic group. The amount of phenolic hydroxyl decreases due to the oxidation of hydroxyl content formed by the cleavage of Ar–O linkages. Due to the difficulty in removing the sulfonic group, its content remained unchanged; however, due to the breakage of carbon–carbon bonds, a decrease in the carboxyl group functionalities was observed. The minimum potential required for this degradation is 2.0 V, while the effective depolymerization was carried out at 2.5–3.0 V. A potential of more than 3.0 V results in the cleavage of the ring. The PbO_2 electrode was removed from the membrane surface as it started to degrade when the current density increased from 10 mA cm^{-2}. By changing the pH, a significant change was also noted, as precipitation of lignosulfonate and electrode corrosion takes place as a result of very low pH.[67]

Furthermore, by modifying the PbO_2 electrode, the lignin EO can be enhanced. Hao et al.[82] synthesized a doped PbO_2 electrode (FeCN–PbO_2) by simply adding the electrochemical redox anion $[Fe(CN)_6]^{3-}$ into the PbO_2 matrix via migration for alkali lignin (AL) degradation. This modified doped electrode shows a higher overpotential for oxygen, a larger surface area, and longer service time as compared to the unmodified PbO_2 electrode. Hao et al.[82] also studied the effects of different experimental parameters, such as the initial concentration of AL, the pH value, the solution temperature, and the applied current. Moreover, no further investigation of the degradation products was conducted as this work aimed to treat the wastewater from industries containing lignin and lower the chemical oxygen demand value.

On the other hand, iridium oxide-based electrodes are regarded as excellent electrode materials for the EO of lignin because of their electrochemical activity and stability, favorable activity toward selective depolymerization of lignin, and dimensional stability as anodes (DSA). IrO_2-based mixed metal oxide anodes (Ti/Ta_2O_5–IrO_2, Ti/SnO_2–IrO_2, Ti/RuO_2–IrO_2, and Ti/TiO_2–IrO_2) for the EO of Kraft lignin paired with a Pt cathode were studied by Tolba et al.[80] It has been observed by various electrochemical studies that the Ti/RuO_2–IrO_2 electrode is a promising catalyst/electrode material for lignin depolymerization offering high stability, high activity, and the highest reaction rate constant compared to other catalysts, while the Ti/Ta_2O_5–IrO_2 electrode shows poor activity for lignin depolymerization due to its large surface area but is considered the most active electrode for OER. Under controlled conditions (a temperature of 60 °C, a current density of 500 mA cm^{-2} and a lignin concentration of 500 ppm), vanillin and vanillic acid were produced.[80]

Other IrO_2-based mixed metal oxide (MMO) electrodes, including the binary oxide coating ($Ru_{0.4}Ir_{0.6}Ox$) and several ternary oxide coatings ($Ru_{0.2}Mn_{0.2}Ir_{0.6}Ox$, $Ru_{0.2}Pd_{0.2}Ir_{0.6}Ox$, $Ru_{0.2}V_{0.2}Ir_{0.6}Ox$, and $Ru_{0.2}Ti_{0.2}Ir_{0.6}Ox$), were studied by Rauber et al.[83] A monomer yield of 11.5% was obtained for lignin depolymerization, which is considered the best performance of the $Ru_{0.2}Mn_{0.2}Ir_{0.6}Ox$ electrode compared to other ternary oxide-coated electrodes. The MMO electrode with composition $Ru_{0.2}M_{0.2}Ir_{0.6}Ox$ has catalytic activity in the following order: M = Mn > Pd > V > Ti, illustrating that the addition of transition metal in the MMO has a significant influence on lignin degradation. The cleavage occurs via β-O-4 oxidative cleavage, forming mostly aromatic monolignol derivatives, particularly 4-hydroxy functionalities such as p-coumaric acid, 4-hydroxy-3,5-dimethoxy acetophenone and 4-hydroxy-3,5-dimethoxy cinnamaldehyde, along with aliphatic chain products. These results demonstrate that the inclusion of non-precious metals in IrO_2-based MMO electrodes enhances selectivity and efficiency for electrochemical lignin depolymerization.

2.1.1.1.2 Metal/metal alloys. Apart from the metals mentioned above, which are commonly utilized as anode materials, other non-precious metals have also been employed for lignin oxidation. Nickel-based electrodes are frequently utilized as an electrode material due to their surface modification to NiOOH under applied anodic potential, which possesses significant catalytic activity and unparalleled benefits over toxic metals, and are cost-effective for lignin depolymerization. Ni^0 is the starting material for the formation of NiOOH; however, this NiOOH phase shows deactivation due to structural modifications under extreme oxidation conditions.[84] To overcome this limitation, carbon-supported Ni nanoparticles and their alloys are commonly used, as carbon supports provide a higher surface area for better dispersion and stabilize the NiOOH form, thus improving the charge transfer and catalytic activity for lignin depolymerization. Movil and co-workers employed non-precious metals and their alloys (Ni/C, Co/C, and NiCo/C) as electrocatalysts through simple solution-based procedures.[85] The alkali lignin (AL) modification via the electrochemical method in an alkaline medium was achieved efficiently by using

these alloy-based electrocatalysts at a lower potential than needed for OER. The group observed that the oxidation products formed from lignin oxidation were irreversible or quasi-reversible and further involved additional heterogeneous charge transfer steps or homogeneous chemical reactions. By analyzing the results, it has been noted that the EO of lignin is often seen as a lower-potential alternative to the OER; however, the comparison between both processes requires careful interpretation. The thermodynamic potential of the OER (1.23 V vs. RHE) does not include significant kinetic overpotentials present on most electrodes.[58,86] However, the EO of lignin is often performed at anodic potentials that are equal to or above the potential needed for the OER at comparable current densities. The primary benefit of lignin oxidation does not arise from a lower anodic potential but instead from modified reaction kinetics and surface adsorption of lignin that may inhibit the side reaction (OER) and shift the current towards lignin oxidation. Therefore, the total cell voltage and energy efficiency are significantly influenced by catalyst composition, desired current density, composition of electrolyte and its pH, and hence cannot be deduced just from thermodynamic potentials. Additionally, because of the oxidation/reduction process of the electrocatalysts, this study reported the non-precious metal electrocatalysts' reversible oxidation behavior. Among these catalysts, Co/C shows multiple oxidation peaks in linear sweep voltammetry (LSV) scans alongside lignin oxidation. It has been observed that these nanoparticles enhance the surface area for electrochemical reactions, which results in improved mass transportation of both educts and products through the catalyst layer. The results showed that the rate for lignin oxidation is greater for the Co/C catalyst, while similar catalytic activity was observed in the case of Ni/C and NiCo/C catalysts. Both the UV/VIS and FTIR spectroscopy studies support the EO of lignin.[85] The IR spectra show a decrease in the peak intensity of the guaiacyl unit and methoxy groups, while a new band appears at 1616 cm^{-1}, highlighting the formation of a carbonyl group due to the oxidation of the hydroxyl group on the guaiacyl unit, thereby producing a carbonyl-containing product like quinone. On the other hand, UV/VIS spectra exhibited a strong absorbance peak at 235 nm, which corresponds to raw lignin or an aromatic component; however, after oxidation, the intensity of this peak decreases, indicating the degradation of the aromatic structure. This work was mainly devoted to determining the efficiency of non-noble metals for lignin oxidation, while the degradation of lignin products was not the primary focus of these studies.

Furthermore, a metal alloy containing a Co core/Pt partial shell was employed as an electrocatalyst by Movil and co-workers[87] for lignin degradation to produce monomeric fractions and low molecular weight products (LMW). Apocyanine and heptane were identified as major products.[87] It was observed that the concentration of these products increased over time, and they were stable during the reaction, which means that they did not decompose or further oxidize into low molecular weight fractions. However, in the beginning, the concentration of some products (for example, 1,4-di-tert-butyl-phenol and 1,3-bis(1,1-dimethylethyl)benzene) first increased

and then decreased over time, exhibiting their further decomposition or oxidation by hydroxyl radicals. Mechanistic studies on this alloyed catalyst were difficult because both the processes, *i.e.*, heterogeneous and homogeneous were in competition with each other. The result indicates that a heterogeneous charge transfer process was involved in oxidizing the lignin fragments on the catalyst surface, while the reaction intermediate underwent a separate chemical reaction in the solution (homogeneous) due to reactive oxygen species (ROS). In summary, electrode potential plays an important role in achieving the specific product more selectively. In contrast to noble-metal-based anodes for OER, the redox-active non-precious metals and their alloys lower the overpotential for lignin oxidation and also produce stable LMW products at comparable current densities; however, mechanistic pathways and reaction complexity indicate that there is a need for improved selectivity and deeper understanding.

2.1.2. Indirect electrochemical oxidation mediated by small molecules. This indirect oxidation process involves a homogeneous redox catalyst mediator, which first oxidizes the lignin, and then this mediator is regenerated on the surface of the electrode through a heterogeneous electron-transfer reaction. The bond cleavage in lignin is fast and irreversible, as the electrolytic mediator system (EMS) transfers the electrons for lignin depolymerization to form stable products and avoid the recombination. This process is mostly used for the oxidation of lignin model compounds. The literature-reported mediator for EO of lignin will be discussed in this section. Sannami *et al.*[88] investigated TEMPO and 4-acetamido-TEMPO as redox mediators for the EO of a lignin model molecule (4-ethoxy-3-methoxyphenylglycerol-β-guaiacyl ether) that has a non-phenolic subunit with β-O-4 linkages. The group noted that electrolytes play an important role in the selectivity between Cγ-carboxylation and Cα-carbonylation of the substrate. In the system containing LiClO₄ and CH₃CN–H₂O as electrolytes, the oxidation of the benzyl group (carbonylation) was favored, and a low yield of Cα-carbonyl (1.9–11.1%) was obtained. However, using dioxane/phosphate buffer, a high yield of Cγ-carboxyl (72.0–93.2%) was attained, along with preferential oxidation of the aliphatic chain (carbonylation). The redox mediator 4-acetamido-TEMPO was used by the group to validate the reason for reaction selectivity. They noted similar selectivity, but the product yield was higher compared to TEMPO.

Lately, by using the same redox mediator (4-acetamido-TEMPO), Rafiee *et al.*[89] electrocatalytically converted the primary alcohols in the substrate. The group observed that Cβ-hydroxyl groups in lignin are selectively oxidized into LMW carboxylic acids. About 30% of aromatic monomers were produced in the electrocatalytic system using oxidized lignin under acidic conditions as a substrate (Fig. 6).

The non-phenolic subunits for selective Cα-carbonylation were investigated by Shiraishi *et al.*[69] using NHPI as a redox mediator. The selectivity toward Cα-carbonylation of the lignin model compound can be substantially improved by adding 2,6-lutidine. High yields of Cα-carbonylation (85–97% and 88–92%) were achieved by EO of monomeric and dimeric lignin model compounds containing β-O-4 linkages. The same group
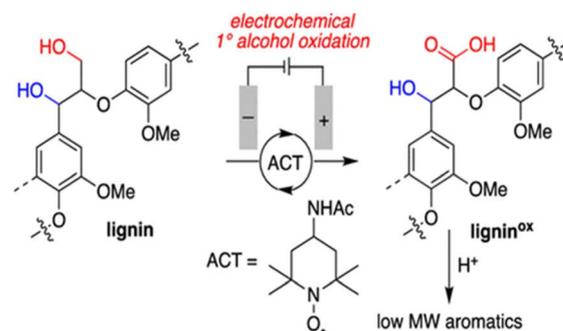

Fig. 6 Electrocatalytic conversion of 1°-alcohol into a carboxylic acid. Reproduced from ref. 89 with permission from *J. Am. Chem. Soc.*, 2019, **141**, 15266–15276. Copyright 2019, American Chemical Society.

reported moderate yields of 5–40% with preferential cleavage of Cα–Cβ bonds using ABTS [2,2′-azinobis(3-ethylbenzothiazoline-6-sulfonate)] as a mediator for the EO of dimeric lignin. In comparison, the conversion of non-phenolic subunits into Cα-carbonyl compounds with high selectivity was provided by NHPI.

In the meantime, using methanol and iodide ions as the reaction electrolyte and redox mediator, respectively, Gao *et al.*[90] studied the EO of the β-O-4 lignin model compound in an undivided reactor. The group noted that the distribution of cleaved products was significantly affected by the electrolytic conditions. By using NaI (60 mol%) as the redox mediator at an applied current of 6 mA, the cleavage of the Cβ–O bond was selectively obtained. A moderate yield of 68% of 2,2-dimethoxy-2-phenylacetaldehyde was obtained by the conversion of the lignin model substrate.

2.1.3. Reactive oxygen species (ROS). This process involves electrical and chemical oxidation reactions mediated by ROS (*e.g.*, H₂O₂, O₂⁻, and ˙OH) produced *via* ORR. These ROS are formed by the *in situ* partial reduction of oxygen, with minor contributions from the reduction of crossover oxygen and peroxide at the cathode as well as the oxidation of oxygen species at high anodic potential. This indirect oxidation is the non-selective pathway of lignin depolymerization, which results in the cleavage of the alkyl aryl ether bond (Caryl–O).[91] In this pathway, the EO of lignin dissolved in the electrolyte occurs directly at the anode, and then this oxidized lignin undergoes chemical oxidation by ROS produced at the cathode.

Zhu *et al.*[92] investigated AL depolymerization by ROS using a simple, non-divided electrolytic cell. The workers employed a graphite felt cathode inside and a RuO₂–IrO₂/Ti anode outside for lignin EO. A high yield of 20 different aromatic products, including vanillin, phenylacetic acid, phenol, other aldehydes, and carbonyl-containing compounds was obtained by ROS-mediated EO. Large amounts of LMW products were acquired by adjusting electrolysis conditions. A high concentration of ROS produced by the decomposition of H₂O₂ and H₂O₂ itself favors LMW product formation. With an external supply of O₂ and 1 hour of electrolysis, a high yield of LMW products was obtained at a surface-normalized current of 8 mA cm⁻² at 80 °C. Both high temperature and current density favor carbon–oxygen
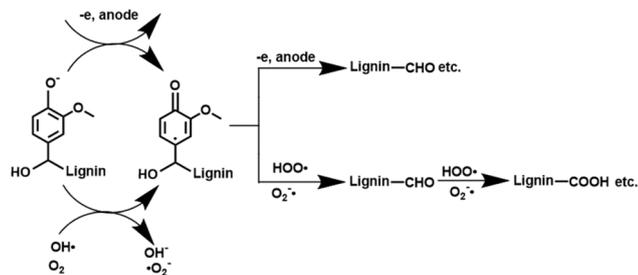
Fig. 7 Electrochemical oxidation mediated by the anode as well as ROS using crude lignin. Reproduced from ref. 92 with permission from *RSC Adv.*, 2014, **4**, 29917–29924. Copyright 2014, Royal Society of Chemistry.

and carbon–carbon bond splitting with the formation of ketones and aldehydes (Fig. 7).

It has been reported by Wang *et al.*[93] that a lignin model compound, *p*-benzyloxyphenol (PBP), was electrochemically degraded by ORR to identify ROS. Wang *et al.*[93] analyzed the superoxide anion radical ($^{\bullet}O_2^{-}$) formed by the single electron reduction of dioxygen. This anion radical ($^{\bullet}O_2^{-}$) is further converted into a hydroperoxyl radical ($^{\bullet}OOH$) by gaining a proton from the lignin model compound (PBP). The as-formed $^{\bullet}OOH$ accepts electrons from PBP and is converted into H_2O_2, which further cleaves the alkyl aryl ether bond (R–O–Ar). The result of this study illustrates that 48.2% PBP is transformed into monomeric products (such as benzyl alcohol, benzoquinone, and benzaldehyde) with a surface-normalized current of 18 mA cm^{-2} at 80 °C for 1 hour (Fig. 8).

A recent study by Ma *et al.*[94] reported that the C_α–C_β bond of the β-O-4 linkages in lignin model compounds is efficiently cleaved by employing EO with *tert*-butyl hydroperoxides (*t*-BuOOH) as a sacrificial oxidant and a platinum anode at room temperature. During electrocatalytic conversion, both the *t*-
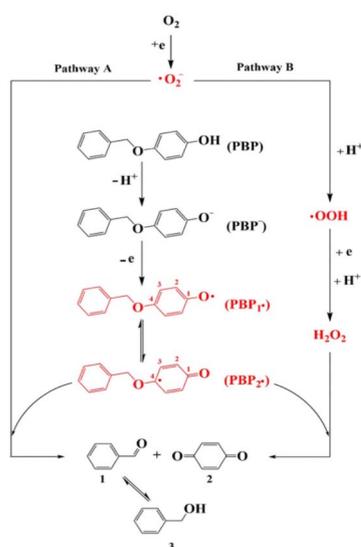

Fig. 8 Schematic illustration of cleavage of the Ar–o–Ar bond of PBP by H_2O_2 formed on the cathode. Reproduced from ref. 93 *J. Electrochem. Soc.*, 2018, **165**, H705–H710. Copyright 2018, The Electrochemical Society.
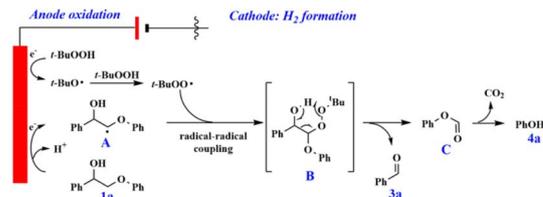

Fig. 9 Possible reaction pathway for the cleavage of the C_α–C_β bond in the β-O-4 lignin model compound. Reproduced from ref. 94 with permission from *ACS Sustain. Chem. Eng.*, 2021, **9**, 1932–1940. Copyright 2021, American Chemical Society.

BuOOH and lignin model compounds are oxidized on the anode and converted into radical A with C_β–H and *tert*-butylperoxy radicals (Fig. 9). Moreover, a peroxide intermediate is formed between radical A and the *tert*-butylperoxy radical by radical/radical cross-coupling, which then leads to C_α–C_β bond cleavage to produce phenol and aromatic aldehydes. The authors also demonstrated that highly selective desired aromatic aldehydes could be achieved by the EO strategy, even with polymeric dimer or pure lignin.

2.2. Solvent-assisted electrochemical oxidation of lignin

Solvents play a significant role in the dissolution process of lignin and permit the interaction between the anode and lignin. Various EO studies reported alkaline solutions (*e.g.*, NaOH and KOH) as electrolytes due to their greater lignin solubility and higher conductivity.[95,96] Nonetheless, the EO of lignin competes with the OER; the actual limitation arises from the kinetic overpotential of OER instead of its thermodynamic potential (1.23 V). Thus, in practical systems, OER usually needs much higher potentials, which strictly restricts the selection of potential windows for selective lignin oxidation in aqueous systems. In this regard, ionic liquids (IL) have emerged as excellent alternatives to aqueous electrolytes for lignin depolymerization due to their thermal and chemical stability, non-volatility, better conductivity, higher lignin solubility, and wider potential window as compared to aqueous media, where OER and HER are largely suppressed.[97]

Although ILs are better than aqueous electrolytes for electrocatalytic applications, very few studies have been reported on them due to their scarcity, high cost, and toxicity issues. Reichert *et al.*[65] explored the EO of AL using protic IL (PIL) triethylammonium methanesulfonate on $Ru_{0.25}V_{0.5}Ti_{0.7}Ox$ as an anode. The electrocatalytic process achieved a 6% yield of guaiacol, vanillin, syringol, *etc.* by oxidizing 5 wt% AL solution within a potential window of 1.0–1.5 V against an Ag pseudo reference electrode. The electrocatalytic performance was due to vanadium, as it facilitated single-electron transfer, while ruthenium and titanium at the anode did not participate in catalysis. This PIL is stable below 1.7 V, and LMW products were only formed at potentials up to 1.7 V.

Recently, Ma *et al.*[98] utilized two types of protic ILs [PrSO$_3$-Hmim][OTf] and [BSO$_3$Hmim][HSO$_4$], and one aprotic IL [Bmim][OTF] for comparative EO of three different lignin model substrates: 4-ethoxyphenol (EP), 4-phenoxyphenol (PP), and veratrylglycerol-β-guaiacyl ether (VG). The ROS produced at the

cathode because of the reduction of oxygen are involved in the indirect chemical oxidation of lignin into *p*-benzoquinone, phenol, guaiacol, and veratraldehyde; the effect is stronger in the case of protic ILs. Additionally, the distribution of cracked products can be controlled by using different types of ILs. The authors noted that electrochemical degradation of lignin was more favorable in protic ILs (H_2O electrolytes) due to low solution resistance and higher conductivity as compared to aprotic ILs. The current efficiency for the electrolysis of VG after 12 h is 88.3% in [PrSO$_3$Hmim] [OTf]–H_2O under oxygen, which is higher than the other two ILs *i.e.*, 85.2% in [BSO$_3$Hmim] [HSO$_4$]–H_2O and 34.1% in [Bmim][OTF]–H_2O. In the work reported by Dier *et al.*[99] two distinct types of ILs, including tri-ethylammonium methanesulfonate (TMS) and 1-ethyl-3-methylimidazolium trifluoromethanesulfonate ([emim][OTf]), representing protic and aprotic solvents, respectively, were used for electrolytic degradation of lignin. The electrolysis was carried out at a cell voltage of 2.5 V and a temperature of 65 °C using a stable glassy carbon electrode surface. By employing GC-MS, several different monomeric and oligomeric products were identified, with yields of 23 and 90 wt% in [emim][OTf] and [TMS], from lignin depolymerization. By using aprotic ILs, including 1-butyl-3-methylimidazolium tetrafluoroborate ([Bmim]BF$_4$), Wang *et al.*[93] performed the degradation of *p*-benzyloxyl phenol (PBP) using RuO$_2$–IrO$_2$/Ti mesh as an anode and porous C-polytetrafluoroethylene as a cathode material. In this experiment, lignin degradation occurred by the attack of *in situ* produced ROS on the ether linkage (Ar–O–Ar) of PBP with the formation of the following degraded products: *e.g.*, benzyl alcohol, benzoquinone, and benzaldehyde.

The primary issue with ILs is their elevated cost, which restricts their utilization in commercial applications. Moreover, substantial water input in the downstream process and higher viscosity during dissolution can create major obstacles for electrocatalytic processes. Certain forms of ILs, particularly those based on imidazole, pose significant toxicity issues; they exhibit low biodegradability, are typically harmful to microorganisms, and can generate hazardous byproducts during hydrolysis.

2.3. Electrochemical oxidation *via in situ* product separation

The major drawback of the EO of lignin is product overoxidation. To overcome this hurdle, a number of product separation methods, including *in situ* methods, were designed to avoid this overoxidation (such as in-line membrane separation and *in situ* extraction).

Stiefel *et al.*[24,100] showed the depolymerization of Kraft lignin using an electrochemical membrane reactor with an *in situ* membrane filtration-based approach for product separation. This filtration method results in higher production of LMW products by preventing overoxidation and facilitating a higher yield. Several Ni-based electrodes, including Ni-wire, Ni-foam, Ni-plate, and Ni-fleece, were studied under galvanostatic conditions (2, 4, 6, and 8 A) by utilizing 1 M NaOH as the electrolyte. The results indicate that materials with increased porosity display diminished mass transfer coefficients (plate >

foam > wire > fleece), which can be attributed to the extended diffusion pathways the substrate must travel to access the electrode surface. Based on the measurements of the molecular mass of the products at various applied currents, it was found that the foam stack electrode caused the most extensive depolymerization, while no bond cleavage was observed with the Ni plate. While various hydrodynamic factors were thought to be responsible for the observed differences, no definitive conclusion was reached. The study reported that over the nickel foam stack, the molecular weight of lignin decreased by 96% in 11 hours at an applied current of 8 A under ambient conditions. The study was conducted fairly and accurately reported the results of identification and quantification. Although, no major product was identified, some of the quantified products included apocynin, vanillin, and syringaldehyde, each with yields of no more than 0.5%. It was still difficult to completely analyze (identification and quantification) the produced LMW compounds (Fig. 10).

To prevent the overoxidation of degraded products of Kraft lignin, an *in situ* product extraction method was designed by Di Marino *et al.*[101] This method involves dissolving lignin in a deep eutectic solvent while isobutyl ketone is used as an extracting solvent. The oxidation of lignin yields an emulsion while simultaneously facilitating the degradation of lignin and recovery of the product. Moreover, the usage of chemical agents considerably raises the costs of the process. The EO process deconstructs and functionalizes lignin into reactive oxygenated intermediates, which are prone to repolymerization and sometimes overoxidation under high potentials. To avoid repolymerization and overoxidation, the integrated ECH process discussed in Section 3 stabilizes these reactive intermediates *via in situ* hydrogenation or hydrodeoxygenation. When viewed together, both EO and ECH processes are complementary electrochemical tools that selectively valorize lignin under controlled mild electrochemical conditions, providing a unified approach for desirable selectivity and minimizing the unwanted side reactions.

3. Electrocatalytic hydrogenation (ECH) of lignin

Generally, lignin-derived bio-oil is the major source of renewable aromatics and sustainable fuels; however, the direct use of
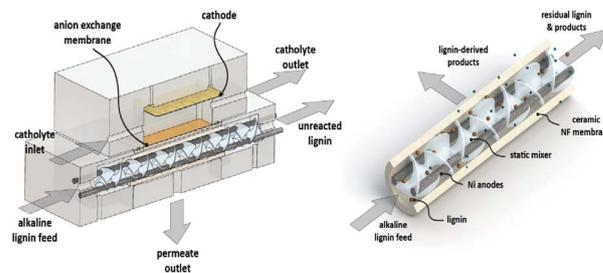

Fig. 10 Scheme of the electrocatalytic membrane reactor. Reproduced from ref. **24** with permission from *Electrochem. Commun.*, 2015, **61**, 49–52. Copyright 2015, Elsevier.

bio-oil is impossible due to some major features such as high viscosity, chemical instability, easy polymerization, high water (15–30 wt%) and oxygen (35–40 wt%) contents, and low energy density as compared to petroleum or crude oil.[102–104] Thus, to use it as an alternative to fossil resources, upgrading and stabilizing the bio-oil is essential to improve its quality.[105] The main objective of bio-oil refining is to improve the energy density by increasing the H/C ratio and reducing the oxygen content in the bio-products. The traditional bio-oil upgrading processes are primarily thermally driven, mainly thermal catalytic hydrogenation (TCH), which is conducted at a high temperature of 200–500 °C and a high H_2 pressure of 100–200 bar (produced from fossil fuels, such as reforming of methane) to attain higher product yields. Due to these severe upgrading conditions, bio-oil is unstable (like aldehydes, furans, and phenolic compounds), and its polymerization increases at 80 °C, which leads to the production of tar and coke, resulting in catalyst deactivation and reactor plugging. In batch systems, catalyst fouling from coke/tar deposition over time causes plugging, whereas in flow systems, coke and tar deposit in narrow flow channels and obstruct tubing or catalyst beds.[42] Therefore, upgrading bio-oil by TCH is an expensive and energy-intensive process; hence, this area still needs groundbreaking research in terms of environmental and economic challenges.

Reductive catalytic fractionation (RCF) is one of the most promising methods and is considered a lignin-first approach for fractionating and upgrading the lignin using redox-active catalysts such as Ru, Pt, Pd, and Ni.[6,25,106–108] RCF uses solvents such as methanol, ethanol, water, cyclic ethers, or their mixtures to extract lignin from LCB at 200–250 °C and 30–50 bar H_2. The extracted lignin is then catalytically hydrogenated and hydrogenolyzed using pressurized or molecular hydrogen in batch systems.[33,109] The initial stage involves the extraction and partial depolymerization of lignin, resulting in unsaturated fragments that are susceptible to repolymerization. Subsequently, in the catalytic phase, the extracted fragments undergo hydrogenation and are further depolymerized via hydrogenolysis.[107] The primary benefit of RCF is its ability to generate a high monomer yield while preserving the integrity of cellulose. According to the Sels group, when RCF is carried out in an autoclave reactor, the yields of lignin monomers and oligomers obtained are nearly equal to the theoretical maximum.[33,109,110]

In contrast to thermochemical catalysis, ECH operates under ambient reaction conditions (atmospheric pressure and low temperature) and is a green (in situ hydrogen generation by utilizing wind, solar, and hydro energy, which are renewable energy sources) and clean process (useful byproducts like hydrogen and oxygen can be employed as a source of fuel for fuel cell applications) for the upgrading of bio-oil or lignin-model compounds. This process uses the chemisorbed hydrogen (H_{ads}) generated from the water/proton reduction. The H_{ads} is subsequently transferred to upgrade bio-oil or lignin derivatives. This process stabilizes aromatic rings, reactive intermediates, and carbonyl groups by removing the oxygen, resulting in the production of cycloalkanes, phenols, and cyclic alcohols. The reaction kinetics and selectivity can be controlled efficiently by altering the electrode material and regulating the applied potential. The procedure is both secure and simple. This method also involves the removal of oxygen from organic compounds, either by hydrodeoxygenation or hydrogenolysis, thus increasing the energy density of the obtained stable products, such as phenol to cyclohexane.

3.1. Mechanistic pathway in electrocatalytic hydrogenation of organic substrates

Formally, the ECH of organic compounds occurs at the cathode while an oxidation reaction or oxygen formation takes place at the anode; this method is exactly opposite to the EO conversion of lignin. The only side reaction that limits the use of this method is the production of H_2 via thermal (recombination of hydrogen atoms due to weak binding energy and hot surfaces) or electrochemical desorption (combination of two adsorbed hydrogen atoms).[111]

The following mechanism presents the possible reaction pathways in the ECH process (Fig. 11).
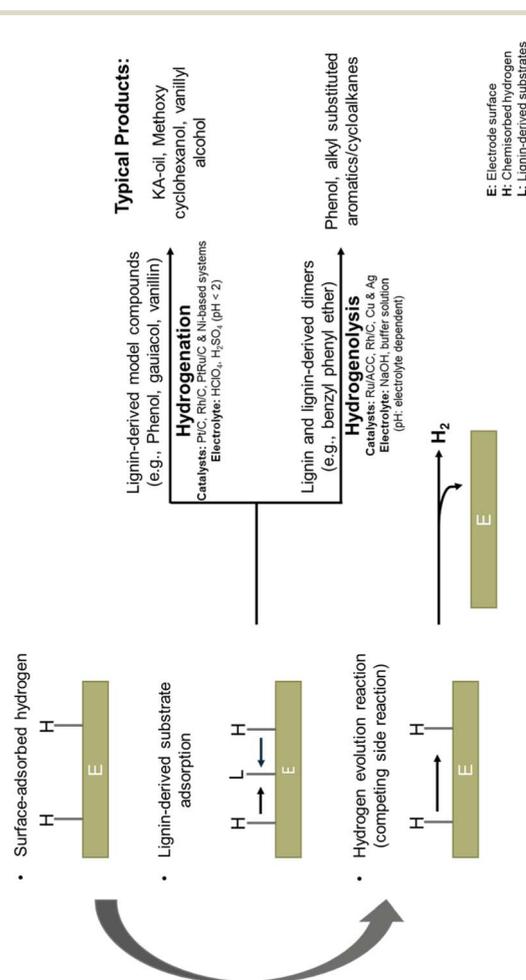

Fig. 11 Schematic illustration of electrocatalytic hydrogenation and hydrogenolysis pathways for various lignin-derived substrates and their possible product distributions, illustrating that the specific pathway is dependent on the nature of the substrate, the catalyst type, and the pH of the electrolyte.

Table 1 An overview of recently published studies on electrocatalytic hydrogenation of lignin derivatives[a]

Substrate	Working catalyst	Electrolyte	ET	I (mA cm^{-2})	T (°C)	Conv. (%)	F.E. (%)	t (h)	Stability	Products	Ref.
Phenol (50 mM)	Pt (2% loading) on Vulcan XC-27R	0.05 M H$_2$SO$_4$	H-cell	40	60	Not reported	85			Cyclohexanol	Amouzegar et al.[118]
Phenol (100 mM)	Pt/C–Pt	0.2 M H$_2$SO$_4$	H-cell	109	50	38.95	82.74	2		76.27% Cyclohexanone 23.73% cyclohexanol	Wijaya et al.[119]
		Catholyte: 0.2 M H$_2$SO$_4$ Anolyte: 0.2 M NaCl				39.52	92.39			74.33% Cyclohexanone 25.67% cyclohexanol	
		Catholyte: 0.2 M H$_2$SO$_4$ Anolyte: 0.2 M NaOH		$E = -0.6$ V vs. Ag/AgCl		17.80	25.49			84.67% Cyclohexanone 15.33% cyclohexanol	
Guaiacol (100 mM)		0.2 M H$_2$SO$_4$	H-cell	109	50	37.88	82.02	2	Retain activity after 4 h of reaction and reuse	19.55% Cyclohexanol 30.44% Cyclohexanone 10.79% 2-Methoxy cyclohexanol 25.46% 2-Methoxy cyclohexanone 9.52% Methanol 4.23% Phenol	
		Catholyte: 0.2 M H$_2$SO$_4$				36.36	93.99			28% Cyclohexanol 16.56 Cyclohexanone 26.79% 2-Methoxy cyclohexanol 18.55% 2-Methoxy cyclohexanone 8.78% Methanol 1.32% Phenol	
		Anolyte: 0.2 M NaCl									
		Catholyte: 0.2 M H$_2$SO$_4$		3.63		16.39	27.33			5.96% Cyclohexanol 29.65% Cyclohexanone 6.93% 2-Methoxy cyclohexanol 20.29% 2-Methoxy cyclohexanone 9.46% Methanol 27.71% Phenol	
		Anolyte: 0.2 M NaOH									
Phenol (20 mM)	Pt/C–Pt	Catholyte: 0.1 M SiW$_{12}$	H-cell	100	35	>99	>98	20 min		87.4% Cyclohexanol 12% Cyclohexane 0.6% Cyclohexanone	Liu et al.[120]
		Anolyte: 1 M H$_3$PO$_4$									

Table 1 (*Contd.*)

Substrate	Working catalyst	Electrolyte	ET	I (mA cm^{-2})	T (°C)	Conv. (%)	F.E. (%)	t (h)	Stability	Products	Ref.
				250	55	>99	90.9	8.9 min		82.9% Cyclohexanol 16.8% Cyclohexane 0.3% Cyclohexanone	
				800	35	>99	95.3	11.3		80.2% Cyclohexanol 18.6% Cyclohexane 1.2% Cyclohexanone	
Guaiacol (20 mM)				100	35	93.5	92.1	25 min		17.4% Cyclohexane 9% Methoxy cyclohexane 50.2% Cyclohexanol 8.7% Cyclohexanone 10.5% Methoxy cyclohexanone 4% Methoxy cyclohexanol 0.3% Phenol	
4-Methyl guaiacol (20 mM)				100	55	77	72	30–60 min		15.6% Methyl cyclohexane 84.4% 4-Methyl cyclohexanol	
Diphenyl ether (20 mM)						84.6	30			6.6% Cyclohexane 23.6% Cyclohexanol 27.2% Cyclohexanone 42.6% Phenol	
Vanillin (20 mM)						91	72			91% 4-Ethyl guaiacol	
Phenol (20 mM)	Ni$_{10}$/MoO$_{2-x}$@C	0.1 M H$_2$SO$_4$	H-cell	$E = -0.7$ V vs. RHE	60	Not reported	53	2	5 cycles	99% Cyclohexanol 1% Cyclohexane	Zhou et al.[121]
	Ni$_{20}$/MoO$_{2-x}$@C			$E = -0.6$ V vs. RHE		Not reported	49			91% Cyclohexanone 8% Cyclohexanol	
Phenol (20 mM)	Ru/ACC	0.2 M HCl	H-cell	40	80	89	29	2.3	2 cycles	99% Cyclohexanol 1% Cyclohexanone	Li et al.[115]
Guaiacol (20 mM)						75	30	3		53% Cyclohexanol 47% Methoxycyclohexanol (36% cis + 11% trans)	
Syringol (20 mM)						58	29	3.8		35% Cyclohexanol 36% Methoxycyclohexanol (27% cis + 9% trans) 13% Methoxycyclohexano-ne 16% Guaiacol	
Phenol (10 mM)	Pt/CC	0.2 M H$_2$SO$_4$	H-cell	100	50	90.2	34.6	1.6		10.5% Cyclohexanone 88.8% Cyclohexanol 0.7% Cyclohexane	Du et al.[116]
	Pt$_3$Ru/CC					96.3	37.6			7.4% Cyclohexanone	

Table 1 (Contd.)

Substrate	Working catalyst	Electrolyte	ET	I (mA cm^{-2})	T (°C)	Conv. (%)	F.E. (%)	t (h)	Stability	Products	Ref.
Phenol (16 mM)	Pt$_3$RuSn/CC					91.5	39.5		8 cycles	91.4% Cyclohexanol; 1.3% Cyclohexane; 2.5% Cyclohexanone; 96.8% Cyclohexanol; 0.7% Cyclohexane	Song et al.[114]
	Rh/C	Acetate buffer (pH = 5)	H-cell	$E = -0.6$ V vs. Ag/AgCl		100	68	3		80% Cyclohexanol; 20% Cyclohexanone	
				$E = -0.7$ V vs. Ag/AgCl	23	100	70	2.5		Cyclohexanone	
4-Methyl phenol (16 mM)				$E = -0.6$ V vs. Ag/AgCl		80	31	3		50% 4-Methyl cyclohexanone; 30% 4-Methyl cyclohexanol	
4-Methoxy phenol				$E = -0.6$ V vs. Ag/AgCl		80	35			50% 4-Methoxy cyclohexanone; 25% 4-Methoxy cyclohexanol	
Phenol (10 mM)	Pt@TiO$_2$	0.1 M H$_2$SO$_4$	H-cell	5	25	Not reported	57		Structural stability	93% Cyclohexanol	Chen et al.[122]
Guaiacol (100 mM)	RhPtRu/CF	0.2 M HClO$_4$	H-cell	50	25	10	62.8	1	40 h (8 cycles)	62.04% 2-Methoxy cyclohexanol; 29.11% 2-Methoxy cyclohexanone; 8.85% Cyclohexanone	Wang et al.[123]
Guaiacol (10–20 mM)	RANEY® nickel	Potassium borate buffer (pH = 8)	H-cell	8	75	<100%	18–26	6	Deactivation over time	Cyclohexanol	Lam et al.[124]
Guaiacol (10 mM)	Pt/CMK-3	0.2 M HClO$_4$	H-cell	20	60	71.2	54.7	1		72.8% Cyclohexanone; 17% Cyclohexanol; 10.2% (Phenol, cyclohexane and 2-methoxy cyclohexanone)	Zhou et al.[125]
	PtNi/CMK-3					11.7	6.3			56.7% Cyclohexanone; 7.9% Cyclohexanol	
	PtNiB/CMK-3					98.9	86.2		20 cycles	54.3% Cyclohexanol; 36% Cyclohexanone; 7.7% (Phenol, and 2-methoxy cyclohexanone)	
Guaiacol (120 mM)	Rh/CF	0.2 M HClO$_4$	Flow cell	300	25	90	64	6	60 h (5 cycles)	65.6% 2-Methoxy cyclohexanol and 2-methoxy cyclohexanone	Peng et al.[126]
Syringol (80 mM)						91	38	5		70.3% Methoxy cyclohexanes	
Guaiacol (120 mM)	PtRh/CF	0.2 M HClO$_4$	Flowcell	200	25		39	1		Not reported	Peng et al.[127]

Table 1 (*Contd.*)

Substrate	Working catalyst	Electrolyte	ET	I (mA cm^{-2})	T (°C)	Conv. (%)	F.E. (%)	t (h)	Stability	Products	Ref.
	PtRhAu/CF					95	58	5	60 h	76% 2-Methoxy cyclohexanol	Yang *et al.*[128]
Guaiacol (25 mM)	Pt/C	Catholyte: 0.25 M PW12 Anolyte: 2 M H$_3$PO$_4$	H-cell	50	60	77	75.1	30	Not reported	27% Cyclohexane 46% Cyclohexanol	
Syringol (25 mM)						52	68.3			18% Cyclohexane 33% Cyclohexanol	
4-Propyl guaiacol (25 mM)					80	82.21	92.19	30		53.44% 4-Propyl cyclohexane 28.72% 4-Propyl cyclohexanol	
						>99	57.91	1		54.27% 4-Propyl cyclohexane 30.08% 4-Propyl cyclohexanol	
Eugenol (25 mM)					80	>99	58.51	1		63.14% 4-Propyl cyclohexane 19.52% 4-Propyl cyclohexanol	
Benzaldehyde (20–180 mM)	Pd/CF	Catholytes: Different proportions of DI-water, alcohol, and acetic acid	Flow cell	50 to 150	25	Not reported	25–100	Not reported	No deactivation	100% Bbenzyl alcohol	Lopez-Ruiz *et al.*[129]
3-Phenoxy phenol (20 ± 4 mM)	Ru/ACC	1 M NaOH	H-cell	33.3	80	100	16	9	Not reported	Cyclohexanol	Garedew *et al.*[117]
4-Phenoxy phenol (20 ± 4 mM)						100	14				
3-Phenoxy toluene (20 ± 4 mM)						67	1				

a ET = electrolyzer type, I = applied current (j = mA cm^{-2}), T = temperature, F.E. = faradaic efficiency, t = time.

The primary factors that affect the efficiency of the ECH process (current efficiency) are chemisorbed hydrogen and the surface coverage of adsorbed organic reactants. Higher surface coverage of organic substrates results in high current efficiency. Usually, with the increase in negative overpotential, the chemisorption of adsorbed H_{ads} on metals increases, as confirmed by H_2 adsorption studies. The drawback at high negative potentials is the formation of H_2, a competitive side reaction that hinders the hydrogenation process. So, an optimal amount of adsorbed H is necessary to efficiently promote the hydrogenation process.

3.2. Electrocatalytic hydrogenation of lignin model compounds

Initial efforts to develop novel reactions and systems utilizing any form of lignin might be difficult due to the intrinsic heterogeneity of this macromolecule. To better understand the upgrading of lignin, model compounds that replicate its characteristic linkages are frequently used.[94,112,113] Most of the studies have explored the upgrading of phenol, guaiacol, syringol, and various other aromatic alkylated compounds, including benzyl phenyl ether, p-cresol, 4-methoxyphenol, and phenolic ethers (Table 1).[114,115] These studies utilized low substrate concentrations (<50 mM) and low current densities (<50 mA cm^{-2}), resulting in low FEs (<50%), making them unsuitable for industrial scalability.[116,117] However, these investigations offer significant insight into catalytic activity, reaction processes, and the impact of functional groups on hydrogenation selectivity. Comprehending the interactions between various metal catalysts and these model compounds facilitates the optimization of reaction conditions for the efficient depolymerization and upgrading of lignin-derived compounds.

A comparative analysis of reported systems highlights that bimetallic and trimetallic systems exhibited better performance (selectivity and FE) than monometallic catalysts and Ra–Ni. Among these multimetallic systems, PtRu/C is a current state-of-the-art catalyst for the hydrogenation of lignin-derived aromatics, while RhPtRu/CF and PtRhAu/CF are the best catalysts for retaining methoxy groups. However, Pt@TiO$_2$, Pt$_3$RuSn/CC and non-noble metal systems like Ni$_{10}$@MoO$_{2-x}$/C are better if higher cyclohexanol selectivity is desired; nevertheless, the Ni-based system serves as a reference system and is a cheap but lower-performance alternative.

3.2.1. Electrocatalytic hydrogenation of phenol. Phenol is the simplest lignin model compound, exhibiting superior selectivity, and high FE, being inexpensive and having better solubility in aqueous media. Thus, investigating its ECH yields insights into the behavior of lignin-derived compounds. Additionally, phenol is also involved in the chemical synthesis of cyclohexanol and cyclohexanone, which are industrially important raw materials for nylon polymers.[130–132] Zhao et al.[133] investigated the reduction of phenol using a Pt sheet as an anode and 1.5 wt% Pt supported on graphite as a cathode in an H-type cell with HClO$_4$ as an electrolyte. The main products of this experiment were cyclohexane and cyclohexanol. Both the cathode material and temperature are key factors that affect the
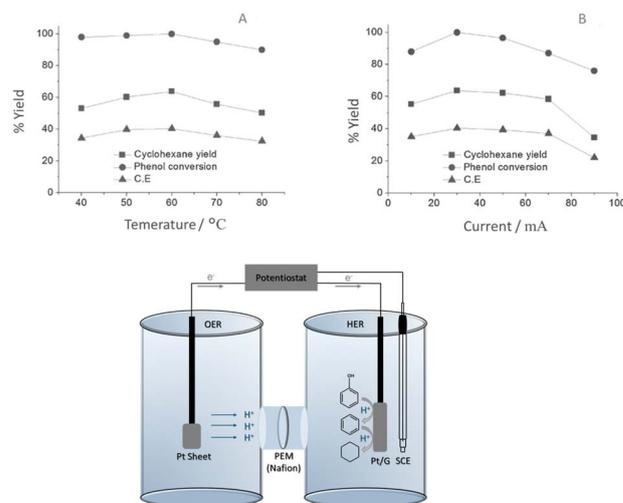

Fig. 12 The effect of temperature (A) and current (B) on the product yield of cyclohexane. The schematic diagram (H-cell) shows how phenol is transformed into cyclohexane on the working electrode. Reproduced from ref. **133** with permission from *Electrochemistry*, 214, **82**, 954–959. Copyright 2014, The Electrochemical Society of Japan.

Table 2 Reaction rates (mol per s g per metal) and TOF (h^{-1}) measured for the phenol hydrogenation on two carbon-supported noble metal catalysts (Pt/C and Rh/C) under distinct reaction conditions. Reproduced from ref. 130

Reaction path	Pt/C		Rh/C	
	Rate	TOF	Rate	TOF
ECH[a]	1.5×10^{-5}	28.8	3.96×10^{-5}	73.5
TCH[b]	6.4×10^{-5}	118.8	2.05×10^{-4}	380.7
ECH + TCH[b]	8×10^{-5}	151.2	2.044×10^{-4}	452.8

[a] ECH was conducted at −40 mA. [b] While TCH was carried out at atmospheric pressure of H_2 without supply of current. Both combined processes (ECH + TCH) were performed at −40 mA with a supply of H_2 at atmospheric pressure. These reactions were conducted in acetic acid (pH = 5) by utilizing 0.05 g of Pt/C and 0.02 g of Rh/C catalysts.

efficiency of the ECH of phenol. Graphite-supported Pt cathodes provide a large geometric surface area (9.5 cm^2) for ECH, resulting in a notable current efficiency of 27.4% and product yields of 44.1% for cyclohexane and 53.9% for cyclohexanol at 20 °C. At the same time, the effect of temperature on product yield was investigated at five distinct temperatures (40, 50, 60, 70, and 80 °C). The cyclohexane yield at 40 °C was 53.2%, which increased to 63.7% at 60 °C. When the temperature was further increased to 80 °C, the cyclohexane yield returned to 50.3%. This showed that phenol hydrogenation was favored between 60 °C and ambient temperature; more bubbles were visible on the electrode surface, highlighting the high desorption rate of hydrogen between 60 °C and 80 °C. The electrolyte composition also affects the current efficiency and product selectivity. The optimum cyclohexane yield was obtained in 0.2 M HClO$_4$ at 60 °C (Fig. 12a). The cyclohexane yield increases when the current density exceeds 30 mA cm^{-2}, but the yield starts to decrease
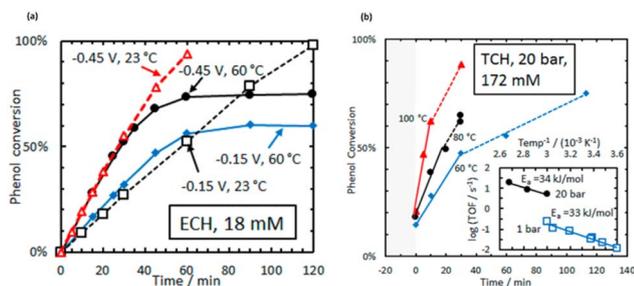
Fig. 13 Conversion profile of phenol: (a) ECH at two different potentials (−0.15 *vs.* −0.45 V *vs.* RHE) using 5 wt% Rh/C catalyst in acetate buffer solution, (b) TCH using an autoclave reactor at different temperatures (60, 80, and 100 °C) under a hydrogen pressure of 20 bar on 5 wt% Pt/C catalyst in water. The inset depicts the Arrhenius plot of the starting TOFs for P_{H_2} at 20 bar (solid black) and P_{H_2} at 1 bar (blue open squares). Reproduced from ref. **134** with permission from *ACS Catal.*, 2016, **6**, 7466–7470. Copyright 2016, American Chemical Society.

Fig. 14 An overview of long-term electrolysis results using (a) $Ni_{10}@MoO_{2-x}$/C at −0.7 V *vs.* RHE and (b) $Ni_{20}@MoO_{2-x}$/C at −0.6 V *vs.* RHE. Reproduced from ref. **121** *Angew. Chem. Int. Ed.*, 2023, **62**, e202214881, under CC BY-NC licence.

when the current exceeds 70 mA cm^{-2} due to electrochemical desorption of adsorbed hydrogen (Fig. 12b).

In a distinct work, Song *et al.*[130] investigated the ECH of phenol under ambient conditions using thermal and electro-catalytic methods. The conversion of phenol was investigated in an H-type cell utilizing Pt/C, Rh/C, and Pd/C catalysts, focusing on the influences of current, electrolyte, catalyst type, and pH. Regarding metal mass and intrinsic activity, Rh/C showed the greatest hydrogenation efficiency normalized to the accessible metal concentration as calculated from turnover frequency (TOF), followed by Pt/C. The Rh/C catalyst achieved the best electrical efficiency of 66.5%, in contrast to 30.5% for Pt/C and 12.5% for Pd/C in H_3PO_4. On these catalysts, the impact of temperature on both ECH and TCH of phenol was also investigated. The estimated activation energies for phenol ECH, based on TOF values, were 29 kJ mol^{-1} for Pt/C and 23 kJ mol^{-1} for Rh/C under mild conditions (5–40 °C). Nevertheless, TCH was carried out without any applied voltage by bubbling H_2 into a solution containing phenol, acetic acid, and a Pt/C catalyst. The activation energy associated with the TCH of phenol under mild conditions (5–55 °C) was 33 kJ mol^{-1}, which closely resembles the activation energy determined for the ECH of phenol. TCH was faster than ECH due to the dissociation of H_2 molecules, which spread over the entire area of the reactor. The two pathways (ECH and TCH) in phenol conversion were independent and followed the Langmuir–Hinshelwood mechanism. In the case of ECH, the chemisorbed H was produced by *in situ* reduction of protons instead of dissociation of H_2 as in TCH. The involvement of evolved H_2 (competitive reaction) in the hydrogenation of phenol was minimal during the ECH process. The sum of the reaction rates and TOF values for the hydrogenation of phenol obtained from separate experiments is equal to that from the combined experiments (Table 2). There is no synergy between ECH and TCH, and both processes are independent (proton reduction, as opposed to re-adsorbed H_2, produces hydrogen radicals for ECH). In both processes, the reaction mechanism follows the same path ($C_6H_5OH \rightarrow C_6H_{10}O \rightarrow C_6H_{12}O$); no C–O cleavage is observed.
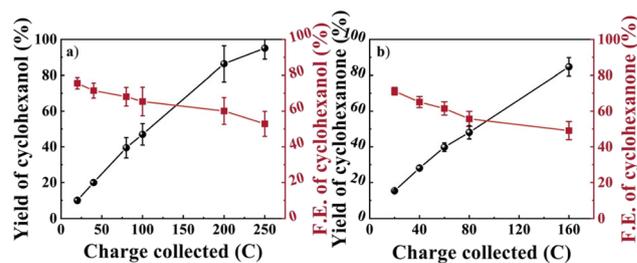
A related study by Singh *et al.*[134] found an unexpected influence of temperature at low cathode potentials (between −0.15 and −0.45 V *vs.* RHE) on the ECH of phenol (18 mM) by using the Rh/C catalyst. The conversion of phenol reached an equilibrium (60–75%) at higher temperatures (60 °C), while at normal temperatures (23 °C), it was nearly 100%. This decrease is due to the dehydrogenation of phenol, which results in the blockage of active sites and lower coverage of chemisorbed H_{ads} at elevated temperatures, as shown in Fig. 13a. This problem could be resolved by boosting the voltage in the electrocatalytic process and increasing the H_2 pressure in the thermocatalytic process (from 1 bar to 20 bar) (Fig. 13b). At high temperatures (60–100 °C), these conditions in both processes remove the blocker site and enhance the surface coverage of adsorbed H, which speeds up the hydrogenation and phenol conversion rates. Comparatively, it was found that the cathode voltage greatly affected the H_{ads} coverage, increasing the negative potentials of the cathode, causing the ECH rates to increase more rapidly than the HER rates at room temperature (23 °C) with a low concentration of phenol (16 mM) and higher
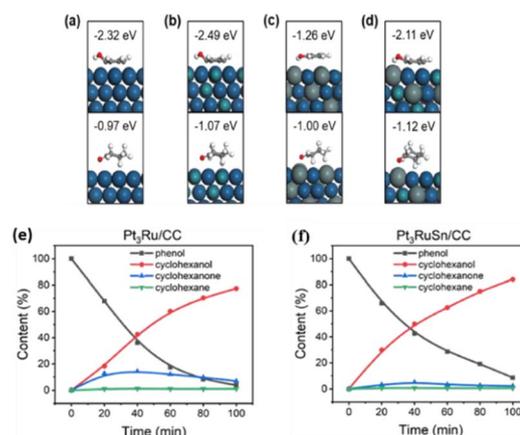

Fig. 15 Distinct adsorption patterns of phenol and cyclohexanone on (a) Pt (111), (b) Pt_3Ru (111), (c) Pt_3Sn (111), and (d) Pt_3RuSn (111). Distribution of reactants and products over reaction time on (e) Pt_3Ru/CC and (f) Pt_3RuSn/CC. Reaction conditions: 0.2 M H_2SO_4 with 10 mM phenol at −100 mA and 50 °C. Reproduced from ref. **116** with permission from *Mol. Catal.*, 2023, **535**, 112 831. Copyright 2023, Elsevier.

cyclohexanol production ($\approx$80 mol%). Under constant potential (-2 V) at the working electrode, the most selective product formed at higher temperatures (30–50 °C) was cyclohexanol using high phenol concentrations (105 mM) by employing 5 wt% Pt/C catalyst and 0.2 M H_2SO_4 as the electrolyte. It is interesting to note that using galvanostatic mode at 50 °C, the product selectivity switched to cyclohexanone, highlighting how the temperature and potential together affect the surface coverage of H_{ads}.[119,135]

According to Zhou et al.[136] the significant overlap between the d-orbitals of Pt and Rh allows the PtRh alloy nanoparticles to have excellent phenol adsorption capability. The H_{ads} produced by the water-splitting reaction on the graphite anode combines with adsorbed phenol on the surface of Pt_1Rh_1 integrated within the mesoporous carbon nanosphere catalyst. The electrocatalyst exhibited exceptional catalytic performance with the highest phenol conversion rate of 95% and an FE of 88%. Cyclohexanol was the major product, with a selectivity of around 66%, followed by cyclohexanone at 34%. Cyclohexanone was then further hydrogenated to produce cyclohexanol. Additionally, Rh incorporation may reduce the metal–H_{ads} interaction, which leads to improved ECH kinetics through the combination of phenol and H_{ads} in the underpotential-deposited hydrogen evolution region (>0 V vs. RHE) with slow HER formation.

Zhou et al.[121] used 0.1 M aqueous H_2SO_4 at 60 °C with Ni–MoO_2/C catalysts to effectively convert phenol into the products. The phenol adsorption on the catalysts was enhanced by the incorporation of MoO_2. The oxygen vacancy (Ov) in MoO_2 can accept electrons from a nearby Ni atom (charge transfer from Ni to MoO_2), enhancing the adsorption of phenol. Cyclohexanol and cyclohexanone were the major products of this conversion. The oxygen vacancy determines the selectivity of the products depending on the different loadings of Ni in the catalyst. Increasing the Ni content in the catalyst structure (Ni_{20}@MoO_{2-x}/C) decreases the oxygen vacancy sites, leading to an elevated yield of cyclohexanone (86%); however, decreasing the Ni content in the catalyst structure (Ni_{10}@MoO_{2-x}/C) enhances the oxygen vacancy sites, which results in an elevated yield of cyclohexanol (95%) and a modest FE of 53% at -0.7 V vs. RHE (Fig. 14a and b). Control experiments indicated that the higher ECH efficiency was due to the heterogeneous $NiMoO_{2-x}$/C (subscript x denotes the missing oxygen atom in the MoO_2 lattice) structure. The two-electron transfer mechanism was associated with Mo in the potential zone before phenol's ECH, as revealed by Fourier-transformed alternating current voltammetry. These experiments suggest that this electron transfer process enhances the oxygen vacancy sites in the catalyst without directly involving the ECH of phenol. The significant interaction between the catalyst surface and the phenol/intermediates was verified by an in situ drift experiment and DFT calculations.

Recently, Yan Du et al.[116] reported different metal- and metal alloy-based catalysts (Ru, Pt, Pt_3Ru, Ru_3Sn, Pt_3Sn, and Pt_3RuSn) supported on carbon cloth for the ECH of phenol. The authors noted that the activation of the phenyl ring was increased by the synergistic effect of bimetallic Ru and Pt, while a new adsorption site for phenol was created by adding Sn. DFT studies revealed that the Pt_3RuSn/CC catalyst exhibits exceptional catalytic activity, producing cyclohexanol with nearly no cyclohexanone throughout the entire reaction process (Fig. 15a–f). The apparent rate constant and activation energy revealed the ranking of the catalysts in the following order: Pt_3Ru/CC > Pt_3RuSn/CC > Pt/CC > Pt_3Sn/CC > Ru/CC > Ru_3Sn/CC. The degree of shift in the linear sweep voltammogram (LSV) upon the addition of substrates is linearly associated with inherent catalytic activity, as confirmed by the kinetic parameters.
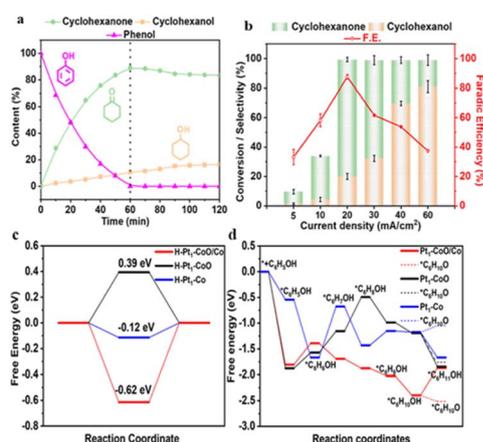

Fig. 16 (a) Variations in the phenol content and its products for ECH over Pt_1–CoO/Co, (b) conversion, product selectivities, and FE of phenol ECH over Pt_1–CoO/Co across a surface-normalized current range of -5 to -60 mA cm^{-2}. (c) Calculated dissociated H free energies, and (d) phenol hydrogenation free energy diagrams on Pt_1–CoO/Co, Pt_1–CoO, and Pt_1–Co surfaces. Adapted from ref. **137** with permission from Inorg. Chem., 2023, **62**, 19123–19134. Copyright 2023, American Chemical Society.
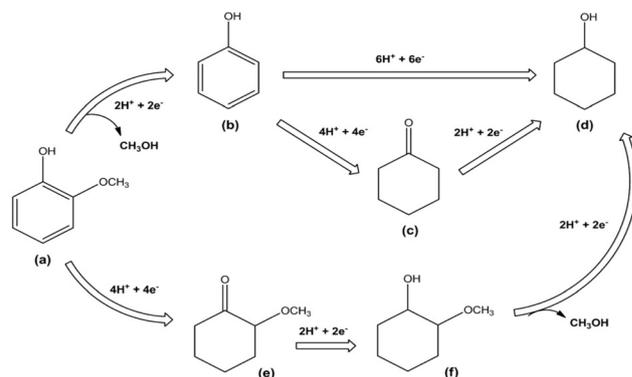

Fig. 17 The reaction pathway for the conversion of guaiacol to cyclohexanol, indicating key intermediates and elementary steps: (a) guaiacol, (b and c) partially hydrogenated intermediates, (d) fully saturated cyclohexanol, and (e and f) methoxy-substituted intermediates involved in demethoxylation. Reproduced from ref. **119** with permission from ChemSusChem., 2020, **13**, 629–639. Copyright 2020, John Wiley and Sons.
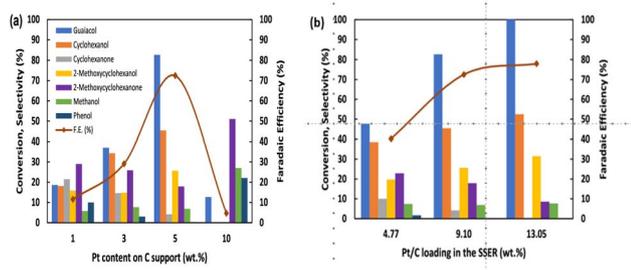
Fig. 18 ECH of guaiacol in a 0.2 M methanesulfonic acid electrolyte under potentiostatic control, illustrating the effects of (a) platinum content on the carbon support and (b) supported catalyst (Pt/C) loading in the SSER. Reproduced from ref. **138** with permission from *ACS Sustain. Chem. Eng.*, 2021, **9**, 13164–13175. Copyright 2021, American Chemical Society.

Tong et al.[137] investigated the synergistic effect of Pt single atoms supported on the CoO/Co heterostructure (Pt$_1$–CoO/Co) for the ECH of LCB-derived phenol in 0.2 M HClO$_4$. The electrocatalyst exhibits excellent catalytic activity at −20 mA cm^{-2} with an elevated conversion rate of more than 99% and a FE of 87.6% towards a mixture of KA oils (cyclohexanone and cyclohexanol). The maximum yield of cyclohexanone, over 80%, was achieved after 1 hour, while the yield of cyclohexanol was less than 20%. Over time, the yield of cyclohexanone diminishes while the yield of cyclohexanol increases in this process (Fig. 16a). Conversely, the increase in current density increases the cyclohexanol content more rapidly, as illustrated in Fig. 16b. This may be ascribed to the increased H_{ads} surface coverage resulting from the higher current density, which enables complete hydrogenation of phenol. However, pure CoO/Co displays negligible reduction of phenol, as also confirmed by electrochemical measurements. DFT studies and experimental results demonstrate that the Pt$_1$–CoO/Co catalyst is responsible for the robust adsorption of hydrogen and phenol, with phenol being activated by the H_{ads} produced on the single-atom Pt sites, resulting in the outstanding ECH of phenol instead of HER (Fig. 16c and d).

3.2.2. Electrocatalytic hydrogenation of guaiacol. Guaiacol (2-methoxyphenol) is a common lignin model compound containing a methoxy group in addition to a hydroxyl group on the
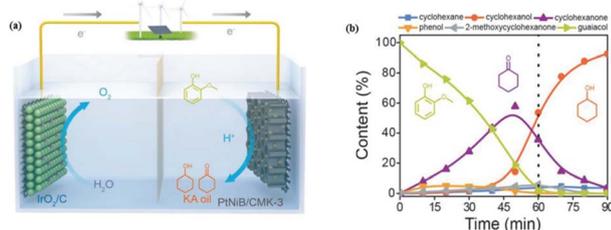
benzene ring. Guaiacol is widely used for ECH studies due to its simpler structure with one methoxy group compared to syringol, which has two methoxy groups. The ECH of guaiacol proceeds through two concurrent reaction pathways: the first route is demethoxylation to produce phenol and then aromatic ring saturation to cyclohexanone, while the second route involves aromatic ring saturation to 2-methoxy cyclohexanone followed by demethoxylation. Both these pathways yield cyclohexanol as the final product upon complete hydrogenation. According to a thermodynamic analysis, the standard potentials of all direct ECH reactions of guaiacol are higher than the HER. The cathode potential and temperature work together synergistically to modify the reaction route, as shown in guaiacol ECH using an agitated slurry reactor.[119,135] A higher temperature (60 °C) enhanced the synthesis of cyclohexanone while suppressing the production of 2-methoxycyclohexanol, indicating the preferred demethoxylation route over ring saturation (Fig. 17). In comparison to the ECH of phenol, the order of reaction for guaiacol hydrogenation was found to be first or second order based on the working conditions, such as temperature, nature of electrolyte, catalyst loading, stirring rates, and concentration of educt. In a slurry reactor, using a Pt/
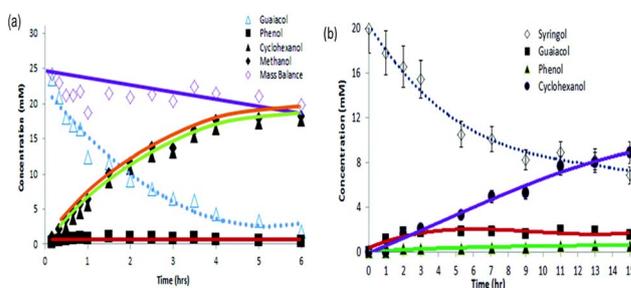

Fig. 20 (a) ECH of guaiacol to cyclohexanol at a current density of 8 mA cm^{-2} and a temperature of 75 °C in a 0.1 M potassium borate buffer; (b) ECH of syringol in a 0.1 M potassium borate buffer containing 0.5 mM cetyltrimethylammonium bromide (CTAB) at 75 °C. Adapted from ref. **124** with permission from *Green Chem.*, 2015, **17**, 601–609. Copyright 2015, Royal Society of Chemistry.

Fig. 19 (a) Schematic representation of the ECH of guaiacol into a KA–oil mixture using PtNiB/CMK-3 as the cathode and IrO$_2$/C as the anode and (b) concentration profile of guaiacol and hydrogenated products over PtNiB/CMK-3. Adapted from ref. **125** with permission from *Adv. Funct. Mater.*, 2019, **29**, 1807651. Copyright 2019, Wiley-VCH.
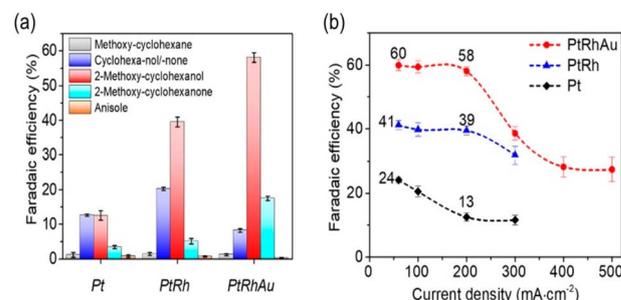

Fig. 21 (a) Faradaic efficiencies for various products employing three catalysts, Pt, PtRh, and PtRhAu, at a current density of 200 mA cm^{-2} for a 1-hour reaction period; (b) FE towards 2-methoxycyclohexanol/none at different current densities for a 1-hour reaction. Adapted from ref. **127** with permission from *J. Am. Chem. Soc.*, 2021, **143**, 17226–17235. Copyright 2021, American Chemical Society.

C catalyst in a current range of 300 to 700 mA and a temperature range of 30–50 °C,[119] whereas the impregnated Ru/ACC employs different ruthenium precursors in a current range of 40 to 160 mA and a temperature range of 25–80 °C,[115] the most common products from the ECH of guaiacol under various conditions were persistently 2-methoxy cyclohexanol and cyclohexanol. Nonetheless, despite the higher current densities, the faradaic efficiencies of the Pt/C catalyst (30–50%) surpassed those of the Ru-based catalysts (8–31%), which is partially ascribed to the configuration of the electrocatalyst.

In another similar study reported by Wijaya et al.[138] a stirred slurry reactor was employed for ECH of guaiacol, with concentration ranging from 20 to 100 mM. The electrolyte consisted of 0.2 M methanesulfonic acid combined with 5 wt% Pt/C (0.10 g) catalyst under moderate reaction conditions, with temperature ranging from 30 to 60 °C. The stirring rate was shown to be crucial because it influences the reaction rate due to mass transport of reactants to the slurry catalyst surface while also facilitating the even distribution of charges across the compartment. After 4 hours at 1 atm and 40 °C with an optimal agitation rate of 350 rpm and an applied voltage of −1.25 V vs. Ag/AgCl with a surface-normalized current of 150 mA, the reaction achieved 73% FE with an 82% guaiacol conversion. In contrast to 1 wt% or 10 wt% Pt, it was shown that 5 wt% Pt enhanced both the FE and guaiacol conversion (Fig. 18a). The total Pt/C concentration also affected the conversion rate; for example, adding 4.8 to 13.1 wt% Pt/C catalyst in the slurry reactor relative to the initial mass of guaiacol (equivalent to a catalyst weight of 0.05–0.15 g) resulted in 48 to 100% conversion (Fig. 18b). At higher temperatures of 60 °C, demethoxylation and ring saturation were facilitated. The group observed that demethoxylation of guaiacol was the slowest process, while the fastest step was the hydrogenation of phenol to cyclohexanol.

Zhou et al.[125] reported ECH of guaiacol and related lignin model compounds such as 3-methoxy phenol, isoeugenol, and eugenol using the PtNiB/CMK-3 (CMK represents ordered
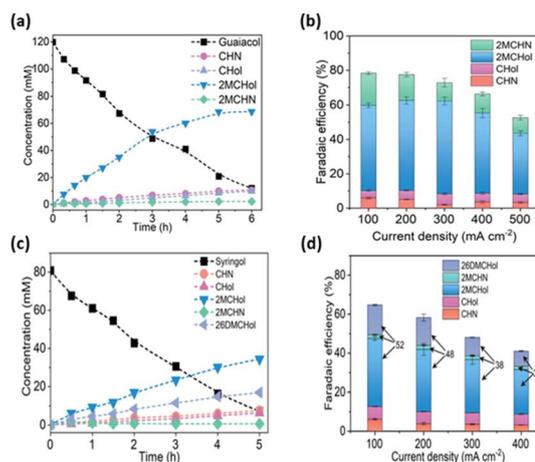
Fig. 23 (a) Time-dependent concentration profile of guaiacol to m-ethoxycyclohexanes at an operating current density of 300 mA cm^{-2}. (b) FEs of products at 100–500 mA cm^{-2} current densities for guaiacol. (c) Time-dependent concentration profile of guaiacol to m-ethoxycyclohexanes with an operating current density of 300 mA cm^{-2}. (d) FEs of products at 100–400 mA cm^{-2} current densities for syringol. Adapted from ref. **126**, *Nat. Commun.*, 2023, **14**, 7229, under CCA 4.0 license.

mesoporous carbon) catalyst as the cathode and IrO$_2$/C as the anode material under mild reaction conditions (20 mA, 60 °C) (Fig. 19a). In this work, the PtNi electronic structure was modified through boron doping. The ECH of guaiacol initially yielded cyclohexanone with a decrease in guaiacol concentration after 50 min; the observed maximum yield of cyclohexanone was 57.7% and decreased over time (Fig. 19b). In the successive step, cyclohexanone was further hydrogenated to cyclohexanol, with the yield increasing slowly in the first 30 min and then reaching a maximum. Remarkably, the boron-doped PtNi/CMK-3 exhibits a high FE of 86.2%, which is 13.7 times higher than that without boron-doped PtNi/CMK-3 (6.3%).

At a moderate temperature of 75 °C and a low current density of 8 mA cm^{-2}, Lam et al.[124] observed electrocatalytic hydrogenation/hydrogenolysis (ECH) of guaiacol into cyclohexanol with a yield of 79% and a current efficiency of 26% over RANEY® nickel electrodes (Fig. 20a). In the ECH process, the cleavage of the ether bond (Ar–OR) is the first step, followed by the saturation of the aromatic ring. The bulky nature of the R-group does not affect the cleavage rate of Ar–OR bonds. Cobalt phosphate catalysts coated on a stainless-steel grid act as an anode and remain workable under constant current for 16 hours, replacing the expensive conventional Pt anode. Syringol was tested for 16 hours with no signs of degradation; the Ra–Ni catalyst lost its catalytic activity due to longer reaction runs (Fig. 20b). As expected, the current efficiency results show that the reactant surface concentration significantly influences the reaction.

Without removing the methoxy group (–OCH$_3$), Peng et al.[127] described the selective ECH of methoxylated monomers generated from lignin to methoxylated chemicals. As this field is growing so rapidly, they haven't yet exhibited the required selectivity because during hydrogenation of guaiacol, it converts
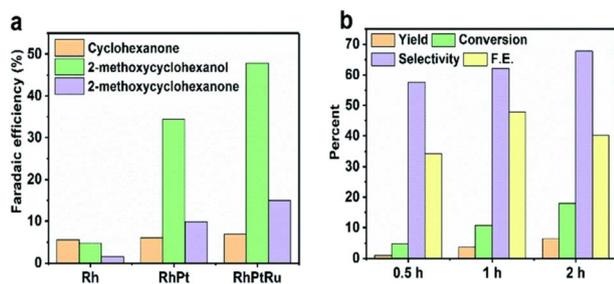
Fig. 22 (a) Bar chart depicting faradaic efficiency (FE) in relation to various catalysts, including Rh, RhPt, and RhPtRu, for the production of different hydrogenated products from guaiacol at a current density of 50 mA cm^{-2} for a duration of one hour during the electrocatalytic reaction. (b) Percentage yield, conversion, selectivity, and faradaic efficiency towards 2-methoxycyclohexanol obtained by upgrading guaiacol utilizing a RhPtRu catalyst at 50 mA cm^{-2} for a duration of up to 2 hours. Adapted from ref. **123** with permission from *Green Chem.*, 2022, **24**, 142–146. Copyright 2022, Royal Society of Chemistry.

into cyclohexanol or cyclohexanone by reducing the desired –OCH$_3$ group. In this study, ternary metal electrocatalysts PtRhAu selectively hydrogenate the lignin-derived monomers to 2-methoxycyclohexanol (Fig. 21a). *In situ* Raman spectroscopy and X-ray absorption spectroscopy confirmed that modifying the electronic structure of Pt by adding Au and Rh into ternary metal alloys affects the energetics of the electrocatalyst surface by promoting guaiacol hydrogenation and preventing the breakage of the C–OCH$_3$ bond. Therefore, a record 58% FE and 200 mA cm^{-2} current density were achieved using guaiacol monomers, representing a fourfold increase in partial current density and a 1.9-fold improvement in FE compared to the highest productivity reported previously. However, when the current density is raised from 300 to 500 mA cm^{-2}, it results in a decrease in FE due to a significant increase in HER at higher currents (Fig. 21b).

Similarly, Wang *et al.*[123] investigated ternary metal RhPtRu catalysts that were supported on carbon felt for the ECH of guaiacol to value-added methoxylated chemicals while retaining the methoxy groups (–OCH$_3$). The developed ternary RhPtRu catalysts achieve a total FE of 62.8% for methoxylated products, including 47.9% FE for 2-methoxy cyclohexanol and 14.9% FE for 2-methoxy cyclohexanone (Fig. 22a). The total selectivity towards these products was 91.2% (29.11% towards 2-methoxy cyclohexanone and 62.04% for 2-methoxy cyclohexanol), from guaiacol, which inhibits the cleavage of the methoxy group (Fig. 22b).

By using a phosphotungstic acid (PW12) electrolyte with NaBH$_4$ acting as a reductant, Han *et al.*[139] investigated the ECH of guaiacol and syringol by employing a suspended Pt/C catalyst. In the case of guaiacol, under an applied current density of 25 mA cm^{-2} at 80 °C, a conversion rate of 75.25% was achieved in 10 minutes. High selectivities of 41.54% and 29.13% towards cyclohexane and cyclohexanone were obtained. However, utilizing the same conditions for syringol, 54.125% conversion was obtained with high selectivity toward cyclohexane (32.21%) followed by cyclohexanol (20.03%). The low conversion rate in comparison to guaiacol is due to the more complicated structure of syringol.

In the most recent study, Peng *et al.*[126] utilized Rh supported on carbon felt for ECH of two lignin-derived model compounds (guaiacol and syringol) in 0.2 M HClO$_4$ (Fig. 23). The reduction of guaiacol produces different keto-alcoholic products, mainly 2-methoxycyclohexanol, 2-methoxycyclohexanone, cyclohexanol, and cyclohexanone. The researchers attained >44% FEs towards methoxycyclohexanes with applied current density in the range of 100–500 mA cm^{-2}. The partial current density of methoxycyclohexanes was around 194 mA cm^{-2} at an applied current density of 300 mA cm^{-2}, which improved to 231 mA cm^{-2} at an applied current density of 400 mA cm^{-2}, achieving a FE of 57.8%. The prolonged electrolysis of guaiacol resulted in a 90% conversion rate and a 59% yield of methoxycyclohexanes at 300 mA cm^{-2} over 6 hours (Fig. 23a and b). When a current density of 300 mA cm^{-2} was applied, the continuous flow cell system maintained 56% FE towards the targeted products for 32 hours. However, the ECH of syringol yielded all products observed for guaiacol with the addition of one more product, *i.e.*, 2,6-dimethoxycyclohexanol. The obtained FEs towards methoxycyclohexanes were in the range of 32–52% at an operating current density of less than 400 mA cm^{-2}. Throughout the 5-hour reaction, the flow cell system displayed a nearly constant full-cell voltage of approximately 3.1 V and achieved a 91% conversion rate with a 64% yield of methoxy-cyclohexanes (Fig. 23c and d).

3.2.3. Electrocatalytic hydrogenation of benzaldehyde. Benzaldehyde is a simple model compound derived from lignin oxidation. It possesses an aromatic ring structure that gives it numerous chemical features similar to lignin-derived compounds. As a representative lignin-derived aldehyde compound, benzaldehyde provides significant insights into how functional groups affect the electrocatalytic upgrading of LCB-derived compounds. The aldehyde functional group affects steric and electronic interactions, leading to weaker adsorption on metal surfaces due to structural distortion. Different carbon-supported metal catalysts were used for the hydrogenation of benzaldehyde, including Pt/C, Pd/C, Rh/C, and Ni/C.[131,140] The
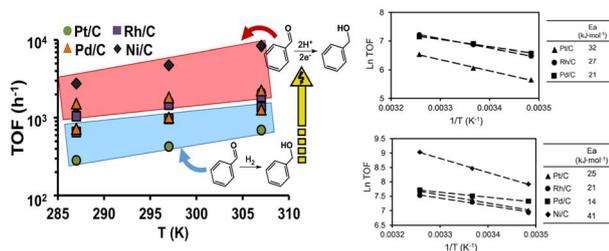

Fig. 24 The catalyst's intrinsic activity in the TCH and ECH of benzaldehyde. Except for Ni/C, which is inactive in TCH, ECH exhibits lower activation energy and higher reaction rates as compared to TCH. ECH conditions: $E = -0.7$ vs. Ag/AgCl for Rh/C, Pt/C, Pd/C, and -0.9 V vs. Ag/AgCl for Ni/C, 1 bar N$_2$, 500 rpm stirring, acetate buffer solution (pH = 5). The reaction conditions were the same in TCH except that no potential was applied and 1 bar H$_2$ was used. Reproduced from ref. 140 with permission from *J. Catal.*, 2018, **359**, 68–75. Copyright 2018, Elsevier.
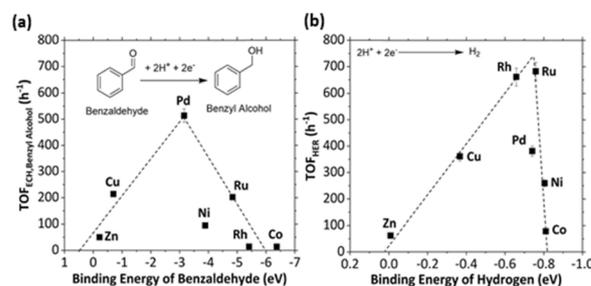

Fig. 25 Volcano plots illustrating the computed binding energies of (a) benzaldehyde to benzyl alcohol and (b) HER with benzaldehyde on precious and non-precious metals. Conditions: $E = -1.15$ V vs. Ag/AgCl, ambient temperature and pressure. The calculated BEs were found with a surface charge of -0.01 e$^-$/surface atoms. Adapted from ref. 141 with permission from *ACS Catal.*, 2019, **9**, 9964–9972. Copyright 2019, American Chemical Society.

interaction of the carbonyl group with the metal is more potent than that of the aromatic ring due to the ring's repulsion from the metal surface, but the overall contact is less. Under the applied conditions, the hydrogenation of benzyl alcohol was not observed because of the hydroxymethyl (–CH_2OH) group, which hinders the adsorption of the ring on the metal surface due to steric and electronic effects. On the other hand, phenol can undergo full ring saturation to cyclohexanone, which then undergoes further hydrogenation to cyclohexanol, presenting a remarkable contrast. So, hydrogenation relies on the functional group (side chains) rather than the aromatic ring. In TCH and ECH processes, the specific substrate–catalyst behavior is responsible for the differing ECH reactivities of phenol and benzaldehyde with different catalysts. Both Pt/C and Rh/C exhibit significant activities for the hydrogenation of both compounds, while Pd shows substrate-selective behavior, displaying higher activity towards benzaldehyde compared to phenol. The observed differences in reactivity were ascribed to the distinct Pd structure: metallic Pd exhibited greater intrinsic activity during benzaldehyde hydrogenation than beta palladium hydride (β-PdHx) during phenol hydrogenation, implying that adsorbed benzaldehyde is more reactive with hydrogen radicals on the three metals (Pd, Pt, and Rh) than adsorbed phenol. For the ECH of benzaldehyde, the activation energy (kJ mol^{-1}) decreases as follows: Ni/C (41) < Pt/C (25) < Rh/C (21) < Pd/C (14). It is noteworthy that Ni/C exhibited activity in ECH although it required a larger cathodic potential (−0.9 V vs. Ag/AgCl) compared to Pd/C, Pt/C, and Rh/C (−0.7 V vs. Ag/AgCl); however, it was inactive in TCH due to the formation of a passive hydroxide layer without applied potential. On the other hand, ECH had higher reaction rates and generally lower activation energies than TCH (Fig. 24).

Reactant coverage, metal composition, and cathodic potential all affect the ECH rates. Increasing the applied voltage boosts the amount of H_{ads} on the electrode surface, leading to greater hydrogenation of benzaldehyde.[134] It is noteworthy that in the case of benzaldehyde, the reaction orders varied depending upon the catalyst, exhibiting zero order on Ni/C and Pd/C and first order on Pt/C and Rh/C. This variation was due to variations in the benzaldehyde coverage, influenced by negative charges generated on the surface by the applied potential. The zero-reaction order suggests that the rapid HER on Ni and the

swift ECH on Pd result in low H_{ads} coverage and high benzaldehyde coverage, respectively. The increase in cathode potential decreases the benzaldehyde surface coverage and increases the reaction order.

Lopez Ruiz et al.[141] investigated the ECH of various oxygenated organic compounds, including benzaldehyde, by employing platinum group metals (Pd, Ru, and Rh) and non-precious base metals (Cu, Ni, Zn, and Co). By using DFT calculations, the binding energies of hydrogen and organic substrates on metals were estimated, which were also utilized to derive the structure–activity correlation for HER and ECH across various potentials. The HER and ECH rates were shown to be correlated with the metals according to the Sabatier principle and were consistent with the binding energies of each respective substrate (atomic hydrogen and benzaldehyde molecules). The substrate–catalyst interaction should be precise with suitable binding strength i.e., neither too strong nor too weak—following the qualitative principles of heterogeneous catalysis. A weak interaction will prevent the substrate from binding to the catalyst, resulting in no reaction; however, a very strong interaction may cause poisoning of the catalyst and inhibit the product dissociation. Based on these correlations, Pd shows optimal binding strength for benzaldehyde, with a binding energy of −3.16 eV, which could account for its superior catalytic activity and selectivity. Conversely, benzaldehyde exhibits moderate binding strength on Cu with a binding energy of −0.70 eV but binds strongly to Ru, with a binding energy of −4.84 eV. Thus, regardless of their positions on opposing sides of the ECH volcano plot, they exhibit similar ECH activity (Fig. 25a). Only the performance of Ni deviated from the expected binding energy with benzaldehyde, while the ECH rate on Rh, Zn, and Co was insignificant. Furthermore, the HER rates also exhibited a volcano-like relationship when predicting the activity based on the binding energy obtained for hydrogen (Fig. 25b). Because of their comparatively strong or weak interactions with hydrogen, base metals are less active than precious group metals, which are still the most active HER metals.

Wu et al.[142] investigated the ECH of benzaldehyde using dendritic-like Pd/Cu-CF-II as an electrocatalyst in 0.1 M H_2SO_4. The self-assembled catalysts were prepared by a two-step electrodeposition process and exhibited low charge transfer resistance (3.7 Ω) and high capacitance (22.9 mF cm^{-2}). The electroreduction of benzaldehyde showed high conversion and FEs of 98.51% and 92.01% with a selectivity of 95.46% towards benzyl alcohol.

The alloying strategy improves the ECH process. Recently, Cheng et al.[143] modified the electronic structure of Ni by alloying it with Pd, resulting in a lower overpotential, high FE, and high electrocatalytic activity comparable to that of pure Pd. Under the applied conditions, the nanoporous nanowires (npnw) $Ni_{82}Pd_{18}$ exhibited a high TOF value of 1387 mol $mol_{metal}^{-1}h^{-1}$ at 100 mV vs. RHE, higher than that of npnw-Ni (60 mol $mol_{metal}^{-1}h^{-1}$) and almost comparable to that of pure np-Pd (1306 mol $mol_{metal}^{-1}h^{-1}$). The increased activity in benzaldehyde hydrogenation arises from the electronic interactions between Pd and Ni which activate the adsorbed

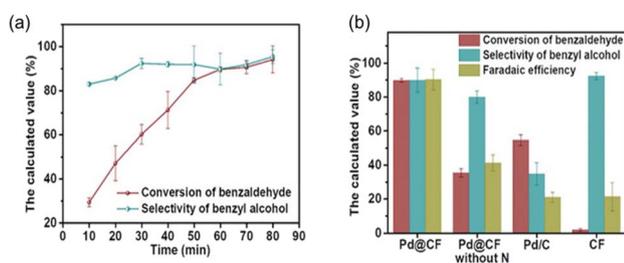**Fig. 26** (a) Reactant and product selectivity profiles using Pd@CF over reaction time at −0.4 V vs. Ag/AgCl, and (b) the conversion, selectivity, and FE employing different catalysts at −0.4 V vs. Ag/AgCl for 60 min. Reproduced from ref. **144** with permission from Adv. Funct. Mater., 2023, **33**, 2214588. Copyright 2023, Wiley-VCH.

Table 3 The conversion of phenolic compounds relative to di-aryl ethers using ECH and TCH under ambient conditions. The reactions of phenolic compounds were carried out in a water–acetic acid mixture, while the reactions of di-aryl ethers were conducted in a water–iso-propanol mixture over an Rh/C catalyst. Adapted from ref. 114

Conditions	Diphenyl ether		Benzyl phenyl ether		p-Tolyl ether		Phenol		4-Methyl phenol		4-Methoxy phenol	
	ECH	TCH	ECH	TCH	ECH	TCH	ECH	TCH	ECH	TCH	ECH	TCH
E (V $vs.$ Ag/AgCl)	−0.9		−0.9		−0.9		−0.6		−0.6		−0.6	
I (mA)	−100		−100		−100		−100		−105		−95	
J (mA cm^{-2})	0.11		0.11		0.11		0.05		0.05		0.05	
R (ECH/TCH)	3.2	4.5	4.7	8.2	2.3	2.8	16	20	8.1	10	7.4	11
TOF (h^{-1})	60	85	88	155	43	50	296	37.4	151	191	138	212
FE (%)	25		36		18		68		31		35	
R (HER)	39		33		42		17		38		32	
t (h)	3	6	3	6	3	8	3.5	3.5	3	3.5	3	3.5

benzaldehyde, as revealed by an *in situ* surface-enhanced infrared absorption spectroscopy investigation.

Recently, Yang *et al.*[144] utilized amine-coordinated Pd nanoparticles on carbon felt as an electrocatalyst for the hydrogenation of benzaldehyde in 0.5 M H_2SO_4. A high conversion of 89.7% with a selectivity of 89.8% toward benzyl alcohol was achieved after 1 hour at −0.4 V by employing Pd@CF (Fig. 26a). Surprisingly, benzyl alcohol showed a high FE of 90.2%, which is much better than the 41.1% for Pd@CF without the N-group and 20.9% for the commercial Pd/C catalyst (Fig. 26b). The amine group (R–NH$_2$) donates electrons to the surface of Pd, which allows more benzaldehyde and H_{ads} to adsorb to the Pd, preventing the HER and improving the overall ECH performance.

3.2.4. Electrocatalytic hydrogenation of dimers. In the last decade, the majority of lignin valorization research was conducted on its model compounds. Only a few studies reported the ECH of lignin dimers compared to lignin monomers.
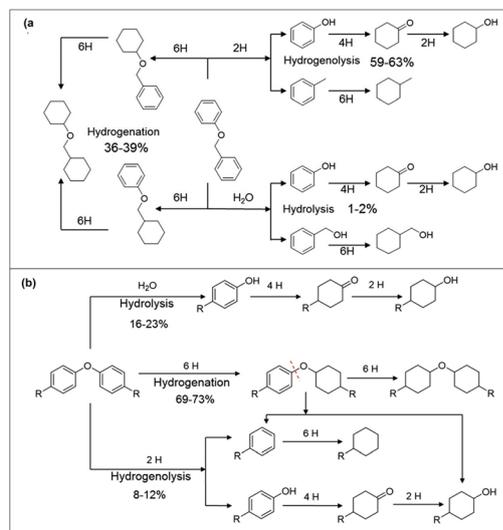

Fig. 27 Reaction pathway for the transformation of benzyl phenyl ether (a) and diphenyl ether and *p*-tolyl ether (b) (where R = H for diphenyl ether and CH$_3$ for *p*-tolyl ether) under ECH and TCH conditions. Adapted from ref. 114 with permission from *J. Catal.*, 2016, **344**, 263–272. Copyright 2016, Elsevier.

Numerous prevalent dimers exist in lignin, based on the linkages between its monomers. For example, diphenyl ether is the most basic structure for the α-O-4 linkage, whereas benzyl phenyl ether is a fundamental structural unit of the β-O-4 linkage. To closely mimic the real structure of lignin, the phenyl hydrogen atoms can be replaced by substituting carbonyl and hydroxyl groups. Dimers containing C–C single bonds, such as β–β, β-1, and β-5 linkages, are exceptionally stable, resulting in poor cleavage reactivity, offering a substantial challenge for lignin valorization. Mahdavi *et al.*[145] reported the ECH of dimer molecules, including benzyl phenyl ether and benzyl methyl ether, under constant current employing a Ra–Ni electrode in aqueous ethanol. To degrade lignin, hydrogenolysis of ether bonds occurred preferentially over aromatic ring saturation. Additionally, HER needs to be suppressed for better ECH. The bond cleavage of the benzyl-*o*-aryl linkage during the ECH required 2 mol of electrons per mole of the substrate.[145] Under galvanostatic control, the product selectivity in the ECH of C–O linkages was evaluated by varying current density, temperature, and substrate concentration. It was found that the product selectivity is unaffected by current density, indicating that ether bond hydrogenolysis predominates over aromatic ring saturation. The HER was suppressed as the current density decreased. At a substrate concentration of 26 mmol L^{-1} and an operating temperature and a current density of 40 °C, and 20 mA cm^{-2}, respectively, both 100% selectivity and current efficiency were achieved. The ECH of two other model compounds, including α-
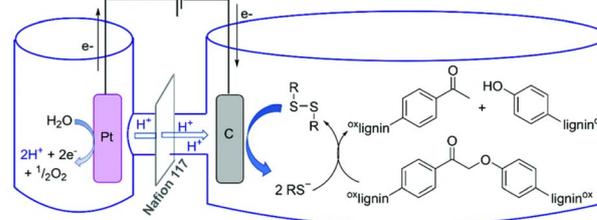

Fig. 28 Potential schematic mechanism of lignin deconstruction in a thio-assisted electrolytic system. Reproduced from ref. 113 with permission from *Green Chem.*, 2021, **23**, 412–421. Copyright 2021, Royal Society of Chemistry.

phenoxyacetophenone and β-phenoxy ethylbenzene, containing C–O linkages, was also studied by the authors under the same conditions.[145] The results indicated that the bond energy for the ECH of C_α–O bond is lower, highlighting the effective hydrogenation compared to C_β–O.

Song *et al.*[114] reported a similar behavior for the conversion of various aromatic ether compounds, including diphenyl ether (DPE), benzyl phenyl ether (BPE), and *p*-tolyl ether (PTE). Both the ECH and TCH reactions were carried out in aqueous isopropanol mixtures over an Rh/C catalyst at atmospheric pressure and ambient temperature.[114] In this study, the aryl ethers' reactivities surged in the following order: PTE < DPE < BPE, and steric effects were also observed. BPE shows the highest reactivity due to the low bond dissociation energy (218 kJ mol^{-1}) of the α-O-4 bond as compared to the 4-O-5 bond in DPE, which required more energy for dissociation (314 kJ mol^{-1}). However, the least reactivity of PTE is due to the steric repulsion caused by methyl groups. The di-aryl ether conversion was always slower than that of phenol and *para*-substituted phenol (Table 3). Depending on the type of substrate, the selectivity varies, as the reaction pathway for the conversion of these aryl ethers is mainly influenced by three different processes: hydrogenation, hydrolysis, and hydrogenolysis. Under both ECH and TCH conditions, hydrogenolysis (59–63%) is the most selective pathway for BPE, while hydrogenation (69–73%) is the most preferred pathway for PTE and DPE (Fig. 27a and b). Nevertheless, the hydrogenation rate is faster (1.6–2.5 × 10^{-5} mol s^{-1} g$_{Rh}$$^{-1}$) compared to hydrogenolysis (4 × 10^{-6}–2.1 × 10^{-5} mol s^{-1} g$_{Rh}$$^{-1}$) and hydrolysis (1–3 x 10^{-6} mol s^{-1} g$_{Rh}$$^{-1}$) rates for all the substrates under ECH conditions, leading to fully saturated products, with the main products being dicyclohexyl ether derived from DPE and cyclohexyl methyl cyclohexyl ether obtained from BPE.

In a recent study by Fang *et al.*[113] the ECH cleavage of the model compound β-O-4 (2-phenoxyacetophenone) was achieved using thiol and reticulated vitreous carbon as the cathode in an H-type cell. In this system, lignin depolymerization was achieved by using disulfide and thiol as redox couples. The reduction of non-phenolic β-O-4 dimers using the disulfide redox couple at 2.5 mA cm^{-2} resulted in a 90% yield of keto and phenolic monomers. Employing the same method, hybrid poplar lignin was cleaved at a higher current density of 10 mA cm^{-2} for 6 hours at room temperature; interestingly, lignin depolymerization was also observed. Aqueous-soluble fragments (26%) and ethyl-acetate-soluble fragments (36%) comprised the majority of the products. Only 38% of the residue was found to be insoluble. In this work, two reaction mechanisms were involved (Fig. 28). One mechanism involved a single electron reduction process for the breaking of the C–O ether bond. In the present case, the electron vector was the disulfide radical anion (RSSR–). The second mechanism depends on oxygen, as O_2 changes the nature of the reaction by removing the electron from the disulfide (an electron-transferring agent). As a result, the conversion rate of 2-phenoxyacetophenone was reduced. The reaction conditions must therefore be closely controlled.

3.3. Electrocatalytic hydrogenation of technical lignin

The ECH of lignin is less common than that of its derivatives. One explanation is that the high efficiency of H_{ads} production in acidic media and the pH needed for lignin dissolution are incompatible. In detail, genuine lignin dissolution is heavily influenced by the alkalinity of the solution, whereas more active hydrogens are produced in acidic media. The HER kinetics in an acidic medium is roughly 2–3 orders of magnitude higher compared to an alkaline medium.[146] The cleavage of O–H bonds in H_2O severely restricts the formation of H_{ads} in alkaline media, resulting in ineffective cleavage of actual lignin by ECH. As a result, these obstacles make it extremely difficult to apply ECH to actual lignin depolymerization. To overcome this, one approach is to change the solubility of lignin by modifying some of its functional groups. Alternatively, more work should be carried out to develop electrocatalysts with effective H_{ads} adsorption and storage properties in alkaline environments. Cruz *et al.*[147] employed levulinic acid, produced during the hydrothermal processing of LCB due to its demonstrated ability to dissolve lignin. Levulinic acid was assessed as a medium for the reductive electrocatalytic depolymerization of the kraft lignin. A copper electrocatalyst was used at −1.7 V *vs.* Ag/AgCl
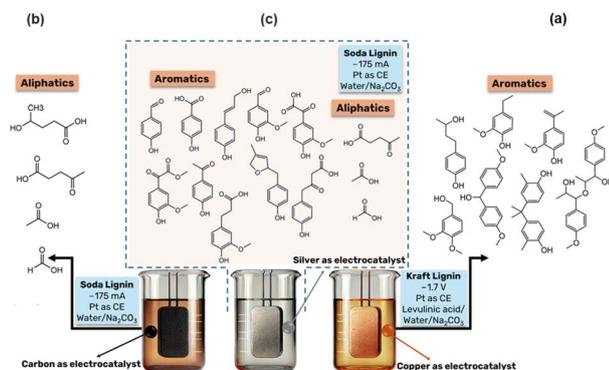

Fig. 29 Comparison of depolymerized products obtained from three studies using an electrocatalytic reductive approach: (a) lignin monomers and dimers, (b) aliphatic products, and (c) mixed aromatic and aliphatic products. Adapted from ref. 149, *Polymers*, 2024, **16**, 3325, under the terms of the CC BY 4.0 license.
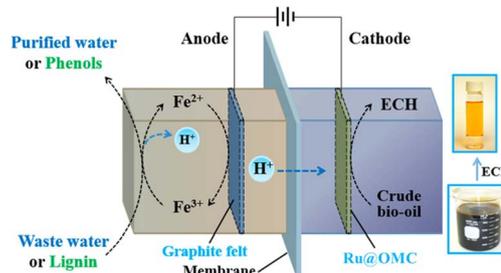

Fig. 30 Diagram illustrating the ECH of bio-oil at the cathode and EO of lignin at the anode. Reproduced from ref. **102** with permission from *ACS Appl. Energy Mater.*, 2018, **1**, 6758–6763. Copyright 2018, American Chemical Society.

© 2026 The Author(s). Published by the Royal Society of Chemistry

for 20 hours because of its economic viability and minimal activity with the HER. The fractionation products mainly include lignin-derived monomers and dimers such as 4-propyl guaiacol, 4-ethyl guaiacol, and 1-phenyl-2-phenoxy-1,3-propanediol, as identified by direct infusion high-resolution mass spectrometry (HRMS) (Fig. 29a). The quantification of these lignin-derived compounds was not reported due to the wide spectrum of compounds identified by MS.

Lindenbeck *et al.*[148] depolymerized and dearomatized the soda lignin to aliphatic compounds using sodium carbonate as an electrolyte and a carbon electrode at −175 mA under ambient conditions. The researchers obtained a 58% yield of depolymerized lignin after 20 hours with four primary aliphatic products, such as sodium formate, sodium 4-hydroxyvalerate, sodium acetate, and sodium levulinate (Fig. 29b). Recently, the same group valorized soda lignin by employing a silver electrode at −175 mA under similar conditions.[149] Initially, the dissolved lignin in sodium carbonate solution has a dark brown color that becomes transparent after 20 hours of reaction. Lignin undergoes partial dearomatization and depolymerization as a result of selective bond cleavage. The aliphatic compounds formed are sodium formate, sodium acetate, and sodium levulinate, while the major aromatic products produced are 4-hydroxybenzoic acid, 4-hydroxybenzaldehyde, and 4-hydroxy-3-methoxybenzaldehyde, as identified by HRMS (Fig. 29c).

The electrocatalytic reductive approach for lignin fractionation prevents overoxidation and unwanted condensation reactions that may arise during lignin depolymerization. These side reactions often result in the generation of recalcitrant compounds that are difficult to valorize.

4. Electrocatalytic hydrogenation of the bio-oil fraction

Fast pyrolysis of LCB in the absence of oxygen produces a mixture of organic products (beyond lignin derived aromatics including acids, furfurals, alcohols, *etc.*) or a liquid called bio-

Fig. 31 Overview of aromatic structure changes resulting from interactions among bio-oil fractions during electrochemical treatment. Adapted from ref. 151 with permission from *Energy Fuels*, 2019, **33**, 11292–11301. Copyright 2019, American Chemical Society.

oil. The bio-oil is renewable and rich in energy and can be transformed into value-added products. However, the direct use of bio-oil is problematic due to its physical and chemical properties, which differ from petroleum crude oil. Bio-oil is more viscous, has higher oxygen (35–50%) and water (15–30%) content, and is less volatile and more unstable because of polymerization than petroleum oil.[103,105] Thus, upgrading bio-oil is necessary to improve the energy density by removing oxygen functionalities (C–O bonds) and increasing the C–C and C–H content. The stabilization and upgrading of bio-oil through ECH experiences numerous challenges, such as complex composition, electrode deactivation, and low current efficiency. Despite these challenges, numerous studies have reported the feasibility and potential of upgrading bio-oil.

Li *et al.*[150] conducted the first ECH study using aqueous bio-oil on Ru-activated carbon cloth (Ru/ACC) as a catalyst. The results indicated that all of the tiny carbonyl (aldehyde and ketone) compounds were hydrogenated to yield their corresponding alcohols and diols, as confirmed by GC-MS analysis, revealing the stabilization of the bio-oil treated by the ECH process. Notably, during electrolysis, the amount of acetic acid in bio-oil drops by 50% because most of it migrates from the cathode compartment to the anode compartment, driven by the attraction between the positively charged anode and the negatively charged acetate anion.

Zhang *et al.*[102] recently proposed a dual-chamber electrolysis cell for the first time to simultaneously oxidize lignin and reduce bio-oil (Fig. 30). They adopted a redox mediator (Fe(III)/Fe(II)) at the anode for lignin ECO to substitute OER, as OER requires high overpotential. Nickel foam coated with ruthenium on ordered mesoporous carbon was employed as the cathode. After 3 hours of ECH, they observed the carbon distribution using a total organic carbon detector and found 0.4% on the membrane, 7.2% on the cathode, and 1.2% lost to volatilization, while 89.7% remained in the cathodic electrolyte as upgraded water-soluble bio-oil. The elemental analysis of aqueous bio-oil revealed a rise in the hydrogen content and a fall in the oxygen content. Furthermore, compared to the initial bio-oil, both the number-average molecular weight (Mn) and weight-average molecular weight (Mw) significantly increased, indicating that hydrogenation was the main process instead of hydrodeoxygenation, as determined by gas permeation chromatography. The difference in alcohol carbon content was 3.5 times higher than the initial level, as verified before and after electrocatalysis *via* GC-MS analysis. The redox mediator (Fe(III)/Fe(II)) greatly increased the FE during the hydrogenation process. Additionally, investigations were also conducted on the anodic side for the kraft lignin depolymerization using Fe(III), achieving monoaromatics with a yield of 11.87%.[102]

Another ECH investigation was conducted by Deng *et al.*[151] on two types of bio-oils made from diluted raw bio-oil: one water-soluble and one water-insoluble. In this reaction, Pt foil and Pt wire were employed as the working and counter electrodes in a beaker-type cell with 0.1 M LiCl solution as the electrolyte. The original bio-oil was precipitated with cold water to separate it into water-soluble and water-insoluble fractions.
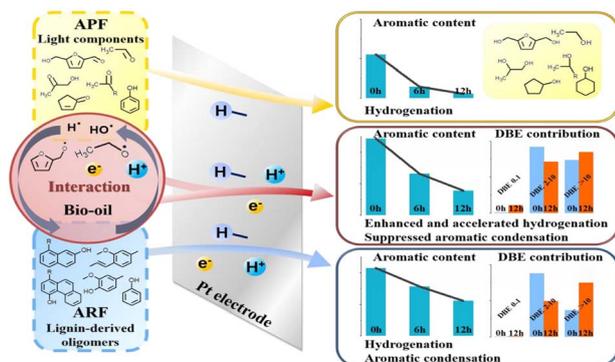
The water-soluble fraction primarily dissolves light molecules from sugars and simple aromatic compounds from lignin, namely the aromatic-poor fraction (APF), while the water-insoluble part contains the aromatic-rich fraction (ARF), predominantly lignin-derived oligomers. After 12 hours of the ECH process, the light constituents of bio-oil primarily experienced hydrogenation under ambient conditions. During the electrochemical treatment, the lignin-derived oligomers underwent both hydrogenation and aromatic condensation. The aromatic content of the entire bio-oil exhibited a more pronounced and quicker fall compared to that in ARF, indicating that hydrogenation was intensified and expedited because of light components derived from sugar fractions in bio-oil (Fig. 31).[151] It is possible that the light organics acted as an organic co-solvent to quicken the hydrogenation of the aromatics. When methanol or ethanol was utilized as a cosolvent, a similar observation was reported in studies using different model compounds.[152]

After a detailed discussion on the ECH of model compounds and bio-oil fractions, it is valuable to contextualize these electrochemical methodologies within the framework of current industrial lignin valorization methods. Among various industrially relevant lignins, the Borregaard process (Sarpsborg, Norway), based on S. Waldvogel's work,[153–155] produces a high yield of vanillin from the valorization of lignosulfonate. This process involves two steps: electrochemical oxidation of lignin followed by thermal treatment to further degrade the oxidized compounds into monomeric products. However, the kraft lignin has also received a considerable attention for its valorization towards the vanillin production. Schmitt et al.[153] utilized Ni- and Co-based electrodes, forming a corrosion-resistant layer of oxyhydroxide (NiOOH/CoOOH) for the electrochemical degradation of kraft lignin. The reaction conditions were optimized by employing 1.9 mA cm^{-2} in 3 M NaOH at 80 °C producing vanillin as the major product with a yield of 1.8 wt% and acetovanillone as a minor product. This work used a highly basic anion exchange resin for the recovery of products from alkaline electrolyte. This adsorption-based recovery avoids the usual acidification and filtering processes that usually cause lignin precipitation and products loss.

5. Advances in electrocatalyst design for the upgrading of lignin derivatives

The rational design of catalysts for the electrocatalytic upgrading of lignin (extending from model compounds to native lignin monomers/dimers and then real lignin) is crucial to evaluate the performance metrics in terms of conversion, selectivity, yield, and FE. Therefore, in this section we provide a detailed overview of recent advancements in catalyst development for lignin valorization. Accordingly, this section not only summarizes the reported catalysts, but it also compares different studies and distills the electrocatalyst design and electrode preparation principles, highlighting strategies that are best for achieving high efficiency in terms of reaction metrics (conversion, selectivity, yield and FE) across different lignin-derived compounds.

5.1. Effects of metal–support interactions

Interactions between metal and support are crucial for controlling adsorption strength, the availability of hydrogen, and stabilizing the intermediates during lignin valorization. Recent research has concentrated on carbon- and oxide-based supported catalysts to improve their electronic properties and inhibit the formation of hydrogen.

Li et al.[115] successfully synthesized ruthenium supported on an activated carbon cloth (Ru/ACC) catalyst through cation exchange (CE) and incipient wetness impregnation (IWI) by employing three different ruthenium precursors for the ECH of guaiacol. In the case of IWI, three different ruthenium precursor solutions (RuCl$_3$, Ru(NO$_3$)$_3$, and Ru(NH$_3$)$_6$Cl$_3$) were prepared, and ACC was immersed in them. Then the wet carbon cloth was dried at room temperature, followed by vacuum drying under the same conditions. The dried ACC was reduced using a H$_2$ pressure of 500 psi at 220 °C in a Parr reactor for almost 12 h. The CE method was used only for the Ru(NH$_3$)$_6$Cl$_3$ precursor. In the typical synthesis procedure, boiling 1 M HNO$_3$ solution was used to oxidize the ACC for 24 h, and then the ACC was washed with deionized water (DI) to remove HNO$_3$ residues, followed by vacuum drying at room temperature. Once the ACC was cleaned, it was immersed in a ruthenium precursor solution containing 1 M ammonia overnight to allow cation exchange onto the ACC. Afterward the ACC was gently washed with DI water, vacuum-dried at room temperature and then reduced under the same conditions as in IWI. The CE catalyst showed superior performance compared to the IWI catalyst, which is attributed to the oxidation pretreatment functionalization of the support surface. The CE catalyst showed a guaiacol conversion of 60% at 25 °C, quite similar to the conversion at 50 °C, while the IWI catalyst showed 15% conversion at 25 °C and 35% at 50 °C. Garedew et al.[156] synthesized Ru/ACC by employing a similar procedure as reported by Li et al.[115] for the ECH of guaiacol using 0.2 M HCl. The group noted 90% conversion in 2 h at 80 °C with a total FE of 33% towards cyclohexanol and 2-methoxy cyclohexanol, showing selectivities of 28% and 17%, respectively.

To improve the catalytic performance, Zhou et al.[157] introduced a PtRu catalyst supported on nitrogen-doped carbon (NDC) for the ECH of guaiacol. The catalyst was prepared in two steps involving carbonization followed by metal coordination with phenolic groups. Firstly, the NDC was produced by carbonizing collagen fiber; KOH serves both as a catalyst for hydrolysis and as a template for carbonization. Then, the platinum and ruthenium precursors were mixed with NDC using tannic acid, which coordinates with metal precursors to form Pt^{4+} and Ru^{3+} that adsorb on the surface of NDC. The obtained catalyst was carbonized in a nitrogen atmosphere for 2 h at 600 °C. With the catalyst featuring abundant defects and edges, the authors achieved 100% guaiacol conversion to cyclohexanol with a selectivity of 78.5% and an FE of 65.4% at 200 mA cm^{-2}.

Carbon-supported Ni–MoO$_2$ catalysts with different Ni loadings (Ni$_{10}$MoO$_{2-x}$/C & Ni$_{20}$MoO$_{2-x}$/C) were reported by Zhou et al.[121] for the ECH of phenol. First, anilinium molybdate was prepared, and then it was pyrolyzed at 650 °C in Ar to make

carbon-supported defective MoO_2 nanowires (MoO_{2-x}/C), which were used as the conductive support. Thereafter, a solution of $Ni(NO_3)_2$ was added drop-wise into the MoO_{2-x}/C solution under stirring. Then the solid $NiMoO_{2-x}$/C was collected *via* centrifugation and dried in an oven at 60 °C overnight. Finally, the catalyst was obtained by pyrolysis at 400 °C in an H_2/Ar atmosphere; Ni nanoparticles were well anchored at the defective sites of MoO_2. The oxygen vacancies (Ov) in MoO_2 accept electrons from Ni, enhancing the adsorption of phenol. The product selectivities depended on Ni loading: the Ov-rich $Ni_{10}MoO_2$/C catalyst adsorbed the cyclohexanone intermediate, promoting further hydrogenation and achieving 95% yield of cyclohexanol, while the Ov-deficient $Ni_{20}MoO_2$/C catalyst desorbed cyclohexanone and favored 86% yield of cyclohexanone at -0.7 V *vs.* RHE.

While carbon supports (carbon cloth, graphene, and carbon nanotubes) are frequently used for catalyst fabrication due to their high electrical conductivity, chemical stability, and large surface area, which are crucial for efficient electron transfer processes during ECH of lignin. However, carbon materials offer limited intrinsic activity, especially the selective hydrogenation or adsorption of polar intermediates. To address these limitations, metal oxide supports serve as excellent candidates by providing additional active sites, tunable acid–base properties, and strong metal–support interaction that improves the catalytic efficiency. Gu *et al.*[158] prepared an Ru/TiO_2 cathodic electrode for the ECH of phenol. The TiO_2 electrode was made using a seed-assisted method, and then Ru species were added to the surface of the TiO_2 electrode through electrodeposition. This three-dimensional catalyst provides microflow channels rich in active sites. The as-prepared catalyst shows full conversion in 40 minutes, with cyclohexanol and cyclohexanone as major and minor products.

These studies highlight the decisive role of support-induced electronic effects in controlling the reaction metrics during the ECH of lignin model compounds. Among Ru-based catalytic systems, Ru/C shows medium to high conversions (60–90%), but it has a low FE (<40%), while bimetallic PtRu/NDC outperforms monometallic Ru/C and is considered the current state-of-the-art catalyst for the ECH of guaiacol, exhibiting full conversion and a comparatively higher FE of more than 60% at industrial current densities. On the other hand, a support with heteroatom (oxygen) vacancies (MoO_{2-x}) exhibited improved catalytic activity by stabilizing the reaction intermediates and making hydrogenation more selective. This comparison shows that altering the metal–support interaction, either by heteroatom doping or by introducing defects, is an excellent approach for lignin upgrading improving hydrogen utilization while suppressing HER.

5.2. Metal/metal alloys

Metals and their alloys have been extensively studied for the ECH of lignin and its model compounds because of their ability to activate the H^+ for reduction, stability under mild conditions, and their high electrical conductivities. Moreover, the synergistic effect of metal alloys tunes the organic adsorption and

improves catalytic performance, especially selectivity, while reducing dependence on costly metals. Cruz *et al.*[45] employed Cu foil as a cathode for the ECH of 2-phenoxyacetophenone in deep eutectic solvent using divided and undivided cells. Various products were formed in both reactors, while β-O-4 cleavage was not observed. Lam *et al.*[124] introduced a RANEY® nickel (Ra–Ni) catalyst produced by the Lessard method for the upgrading of alkoxy lignin model compounds. Nickel was electroplated onto a stainless-steel mesh to make the Ra–Ni cathode by trapping Ni–Al alloy particles. Then, the nickel surface was activated by etching the aluminum using NaOH solution at 75 °C, producing a porous skeletal nickel surface. The highest current efficiency of 26% was observed for cyclohexanol from guaiacol, with a conversion rate of 79% after 6 h. The electrode loses its catalytic activity over extended experimental operation.

The incorporation of a third element into a bimetallic system alters the electronic environment of the catalytic centers, thereby modifying the adsorption strength of organics, and promoting high activity and selectivity.

Peng *et al.*[159] synthesized a ternary metal alloy by doping Au into PtRh using a co-electrodeposition method. The deposition was conducted by performing 50 cyclic voltammetric cycles at a scan rate of 100 mV s^{-1} with an applied potential of -0.5 to -1.7 V. The synthesized catalyst was tested for ECH of guaiacol, aiming to suppress deoxygenation and favor the methoxylated product (2-methoxy cyclohexanol). The Pt and PtRh catalysts exhibited higher Tafel slopes of 150 and 280 mV dec^{-1}, while PtRhAu showed 100 mV dec^{-1}. The group noted that the incorporation of Rh into Pt improves the selective hydrogenation of the ring towards 2-methoxy cyclohexanol. However, further doping of Au into the PtRh catalyst increases the FE of the desired product by suppressing deoxygenation. Subsequently, Wang *et al.*[123] reported similar work in which they developed an RhPtRu catalyst on carbon felt using the electrodeposition method to facilitate the ECH of guaiacol into m-ethoxylated products. The deposition was performed using a similar method as reported by Peng *et al.*[159] In this system, Pt and Rh provide strong adsorption sites for the guaiacol molecule, while the addition of Ru in the ternary catalyst suppresses the competitive HER. The optimized catalyst attained a high FE of 47.9% towards 2-methoxy cyclohexanol, with an overall selectivity of 91.2% for 2-methoxy cyclohexanol and 2-methoxy cyclohexanone.

Heteroatom-doped metal alloys have been investigated to improve the catalytic performance for the upgrading of lignin monomers to high-value products. Zhou *et al.*[125] introduced a boron-doped PtNi alloy supported on ordered mesoporous carbon (PtNiB/CMK-3) through a synthetic reduction procedure. The catalyst was synthesized by dispersing CMK-3 with Pt and Ni precursors in water; then NaBH$_4$ was added dropwise, followed by heat treatment at 140 °C under an N_2 atmosphere. After filtration, the resultant PtNiB/CMK-3 was vacuum-dried at 60 °C. The boron doping into the PtNi alloy optimizes the electronic structure by enhancing the adsorption of reactants and intermediates, thereby increasing the catalytic activity. The PtNi/CMK-3 catalyst without B-doping achieved less than 18% conversion after 2 h, while the PtNiB/CMK-3 catalyst attained

98.9% conversion in 1 h. The observed FE on PtNi-CMK-3 and PtNiB-CMK-3 was 6.3% and 86.2% towards cyclohexanol and cyclohexanone in 1 h.

Recently, Du *et al.*[116] reported the synthesis of a Pt_3RuSn alloy *via* a simple impregnation–reduction procedure to grow nanoparticles onto carbon cloth for the ECH of phenol. Pt, Ru (3 : 1), and Sn precursors were sonicated for uniform mixing. Next, the carbon cloth (CC) was immersed in the solution and subsequently dried at room temperature. The dried CC was reduced under H_2 for 2 hours at 400 °C and passivated under argon. The bimetallic Pt–Ru interaction promotes the hydrogenation of the aromatic ring; however, the introduction of Sn into the PtRu system forms a new adsorption site for the ketonic intermediate, thus achieving 91.5% conversion with 96.8% selectivity towards cyclohexanol.

Metal alloys show superior catalytic performance for lignin-derived aromatics than a monometallic system due to their combined synergistic electronic properties by optimizing the adsorption strength and inhibiting the competitive HER. The monometallic systems (Cu-foil and Ra–Ni) offer moderate conversion, limited product selectivity, and low FE, hindering their upscaling for practical applications. Compared to monometallic systems, metal alloys such as bimetallic and trimetallic alloys exhibit excellent catalytic performance by modifying the adsorption strength for both organic molecules and hydrogen. The doping of a third heteroatom or metal into a bimetallic system enhances the synergistic effect through fine-tuning of the electronic properties, thereby improving selective hydrogenation by inhibiting deoxygenation and hydrogen formation. Interestingly, ternary alloys have emerged as effective catalysts, exhibiting almost full conversion with a high FE of ≈85% or above in a short reaction time. In short, metal alloys are promising candidates for the efficient valorization of lignin derivatives.

5.3. Electrode preparation strategies

In the broader context of electrocatalysis, there are three commonly employed methods for the preparation of electrocatalysts or electrode materials, such as impregnation (dry and wet impregnation)/chemical deposition, electrodeposition, and suspension/slurry formation.[114–116,119,159] The impregnation method involves depositing a catalyst ink solution by drop casting or spray coating onto the porous conductive substrate (such as foams, carbon cloth, and carbon paper); this procedure is known as a coating technique or incipient wetness impregnation. Conversely, immersing the conductive substrate in the precursor solution to fully saturate the porous structure, a process known as cation exchange (CE) or wet impregnation. After saturation, the electrode is reduced using a reducing agent such as sodium borohydride ($NaBH_4$) or a H_2 pressure of 500 psi at 220 °C.[115] Another strategy to design an electrode is mechanical mixing or hot pressing, where the catalyst powder is pressed onto the conductive support using heat and pressure.[145,160]

The electrochemical methods for electrode preparation are electrodeposition and electrophoretic deposition; the former involves the deposition of metal nanoparticles or metal alloys on a conductive substrate by applying potential or current, while the latter involves the charged catalytic particles deposited on the conductive material under the influence of an electric field applied between two electrodes. The slurry suspension is quite recent and well utilized in ECH of lignin model compounds and monomers; the process uses a dispersed catalyst in the electrolyte solution under strong agitation so that the catalyst collides with the conductive substrate to exchange the electron. Each electrode preparation method has its own advantages and limitations. The impregnation method allows good control as the reaction occurs on the electrode surface; however, the thick catalyst layer results in higher charge transfer resistance, and all the active sites are inaccessible. In the electrodeposition process, a smooth film is formed; however, it is not possible to achieve a higher loading of the catalyst. The suspension method provides a large catalytically active surface area for organic conversion by overcoming the diffusion limitations; however, a large catalytically active surface area also promotes the formation of H_2. Furthermore, the process becomes more complex because catalyst particles must collide with conductive electrodes for electron exchange, and catalyst separation and recovery are also challenging, which are simpler in coated configurations.

The electrode preparation methods are decisive in terms of accessibility of catalytic sites and charge transfer resistance to enhance the electrocatalytic efficiency for lignin valorization. The most widely used strategies are coating and impregnation because of their simple operation and easy regeneration of the catalyst; however, higher catalytic loadings might block the active sites and increase the charge transfer resistance. In contrast, electrodeposition results in a uniform layer of the catalyst that shows good adherence on the conductive support; however, this method suffers from low catalytic loadings. Slurry-based suspension systems offer a higher catalytic surface area and better mass transportation, which can increase conversion rates, but they show higher hydrogen formation, difficult-to-regenerate catalysts, and complex operation conditions. Recent research shows that immobilized configurations or electrodeposition generally offer high catalytic performance, operational simplicity, and suitability for practical applications.

6. Challenges and perspectives in electroorganic synthesis

Electrocatalytic lignin valorization is a potential method for producing fine chemicals and fuels from LCB with low sustainability metrics. The *in situ* production of oxygen and hydrogen from water serves as the competitive side reaction, while the electrode-generated reactive species, such as H_{ads}, and ·OH, drive the electrochemical lignin conversion. For the depolymerization of lignin, EO is adapted to increase the oxygen content in the products, whereas ECH is used to boost the hydrogen content for upgrading bio-oil or lignin derivatives.[161] The EO of technical lignin is more common than that of lignin model compounds because the EO process only degrades the

lignin *via* oxidative cleavage and is not involved in chemical synthesis. Moreover, the ECH process can be adapted to depolymerize technical lignin using mixed organic and aqueous solvents. However, it requires superacid catalysts and high temperatures to enable hydrodeoxygenation reactions to remove water. These circumstances are not ideal for ECH pathways, as these components are already present in thermochemical processes. Thus, degradation is achieved by EO, and chemical synthesis is achieved by ECH. Both EO and ECH are complex processes and face several challenges.

• First of all, for EO, the majority of lignin depolymerization reactions are conducted in alkaline media, and the stability of electrode materials (Ni/C, NiCo/C, and PbO_2) is always questionable due to their dynamic nature.

• It is quite challenging to deduce the reaction pathway, as one needs to perform *in situ* or *operando* methods to analyze the reaction intermediate or transient species.

• There are no established protocols in electrochemistry to conduct the reactions in the most precise manner, as there are too many parameters involved both technically as well as chemically.

• Upscaling these reactions would be a problem.

• Catalyst design could be crucial, as catalysts' responses to certain reactions (reduction or oxidation) can differ significantly.

• Product isolation and separation are not trivial.

Various factors like the temperature, pH of the solution, electrolyte type, electrocatalyst, conductive substrate, and the structure of the lignin substrate play crucial roles in improving the overall efficiency of this process.

6.1. Role of electrolyte and current density in electrochemical processes

One of the most substantial factors in lignin depolymerization and upgrading is the selection of an appropriate solvent, which has an impact on the conductivity and solubility of the lignin. Lignin and its derivatives with low molecular weight and low substrate concentration are soluble in aqueous acids and electrolytes, and the majority of the electrochemical studies utilize aqueous electrolytes; however, their solubility decreases with the increase in molecular weight and substrate concentrations. As more oxygen is removed from the reactant, solubility challenges also arise, causing hydrophobic layers to form in the reaction media. The electrolyte conductivity, substrate conversion, and current efficiency are all greatly decreased by this phase separation since it restricts both mass and electron movement. While the phase separation is beneficial for the product recovery in many systems (*e.g.*, the Baizer process),[162] in the case of ECH of lignin, it restricts the diffusion of the substrate to the electrode surface. However, lignin and its model compounds are soluble in organic electrolytes (such as isopropanol, acetonitrile, and acetone), but these organic electrolytes also have poor conductivity, which affects electron transfer and ion movement. Most of the studies utilize a combination of conductive organic and aqueous electrolytes to perform effective ECH of bulky substrates. Nevertheless,

lignin is easily soluble in alkaline electrolytes, which results in the breaking of ether bonds and disruption of the network, but alkaline electrolytes are not suitable for ECH, as lignin is prone to deprotonation in basic media. Thus, considering the energy efficiency, solubility, and product recovery, deep eutectic solvents (DES) and ionic liquids (ILs) are the most effective solvents for lignin. Furthermore, their exceptional biomass fractionation capability offers a workable route to integrating a one-pot lignin electrochemical fractionation approach. However, there is a need to resolve the viscosity problems for ILs and DES. In terms of lignin depolymerization effectiveness, current density is also crucial. For example, high current density may cause overoxidation of products along with the formation of H_2 and O_2, while low current density could lead to ineffective depolymerization. This results in higher CO_2 emissions and lower FE. The FE depends upon substrate concentration and applied current density. Garedew *et al.*[117] noted that FE rises by 25% when increasing the concentration of 3-phenoxy phenol from 10 mM to 40 mM, and by 96% when the applied current density was decreased from 100 mA to 20 mA. Hence, for large-scale applications, both an optimum current density of more than 100 mA cm^{-2} and a high reactant concentration are essential.

6.2. Development and design of electrocatalysts and reactors for improved electrosynthesis

The electrocatalytic depolymerization of lignin through oxidation utilizes both noble (Ru, Au, and Ir) and non-noble metals (Pb, Ni, and Co) and their alloys (PtCo, NiCo, and RuIrPd), while the ECH of lignin and its model compounds greatly depends on precious metals (*e.g.*, Pt, Rh, and Ru) to attain high efficiency and stability. However, the release of greenhouse gases during the extraction and refinement of these metals poses significant environmental issues.[115,156] Non-precious metals release 10 kg CO_2 per kg, which is less than that of platinum (12.5 t CO_2 per kg).[41] Non-noble metals (such as Ni, Cu, Mo, and Co) are attractive choices in this regard due to their low cost and capacity to reduce greenhouse gas emissions. These metals show promising activity for some lignin model compounds, but their performance for different substrates under various reaction conditions still needs to be explored.[141,163] The majority of these noble metal catalysts were used in aromatic ring saturation or hydrogenation reactions due to their intrinsic properties and lower propensity for deactivation under acidic conditions, but scarcity limits their use. To overcome this issue, either doping of transition metals along with noble metals or metal alloys is the best option for the reduction of the complex lignin network structure. However, support materials, particularly carbon-supported catalysts, play a significant role in the conversion and efficiency of the process by improving the dispersion, surface area, mass transport, and conductivity. A comprehensive analysis is required to elucidate the reaction mechanism, assess the influence of different support materials, and evaluate catalyst stability and reusability following oxidation or reduction reactions. The stability of catalysts under electrochemical operational conditions depends on various factors, including the aggregation and loss of metal nanoparticles, the

polymerization of organic substrates, the deposition of impurities on the catalyst, and the large ohmic resistance offered by gas bubbles due to HER or OER at high current density. Reactor design is another challenging factor for lignin conversion. Most of the electrochemical studies on lignin valorization have been conducted on H-type cells, which have a large electrode gap and membrane barriers. These barriers can cause problems like high ohmic resistance and voltage loss, as well as problems in managing gas evolution (HER and OER from competitive side reactions). Moreover, mass transfer limitation is another factor for such cells, as it creates a concentration gradient due to limited stirring, making it difficult for the substrate to reach the electrode surface, which results in low conversions and uneven product distributions. Additionally, transferring H-cells to industrially relevant flow cells is quite challenging, which greatly enhances the economic burden on the industry for commercial applications. A flow cell or zero-gap flow cell electrolyzer has been recommended as a way to decrease the inter-electrode gap and increase energy efficiency. For electrochemical lignin conversion, a zero-gap flow cell is more advantageous than a conventional flow cell due to low ohmic resistance, improved catalyst utilization, minimum product crossover, and operability at higher current densities. Nevertheless, more research is needed to develop high-temperature reactor designs for real lignin depolymerization.

6.3. Membrane technologies for lignin valorization

Membranes represent a trade-off in electrochemical reactors: they prevent crossover and allow different electrode environments, and they are useful if products need to be re-reduced or pH must differ. However, membranes introduce additional ionic resistance, increase cost, and pose fouling risks; therefore, undivided cells are often preferable when crossover or re-reaction is not a problem. Since lignin depolymerization and upgrading are often irreversible, approaches without a membrane could be promising. However, both batch (H-cell) and continuous flow (flow or zero-gap cell) reactors utilize a membrane to separate both anodic and cathodic products. Typically, three different types of ion exchange membranes have been used in the literature, namely anion- and cation-exchange membranes (AEMs & CEMs) and bipolar membranes (BPMs). Both AEMs and CEMs transport anionic and cationic species like OH^- and H^+, while BPMs are laminated AEMs and CEMs that operate in forward or reverse bias, resulting in H^+/OH^- recombination at the membrane junction or water dissociation into H^+ and OH^- at distinct electrodes. For lignin oxidation in basic media, AEMs are commonly used to transport OH^- and maintain the high pH of the solution. However, research is shifting toward the ECH of lignin, which utilizes acidic or slightly acidic conditions. In this regard, CEMs, particularly perfluorosulfonic acid (PFSA)-based membranes such as Nafion, are gaining significant attention within the scientific community. This transition towards CEMs significantly improves thermal and chemical stability, proton conductivity, long-term durability, and resistance to organic fouling.

7. Conclusions and outlook

The electrochemical conversion of lignin (*via* reduction or oxidation) has been extensively studied to produce chemicals and biofuels, which are alternatives to their fossil-based counterparts. The biochemicals and bio-fuels produced by electrocatalytic valorization of lignin or its model compounds offer a sustainable and biobased route. The electrocatalytic depolymerization and upgrading of lignin is conducted under ambient conditions, avoiding the use of high temperature and pressure that is related to thermal catalytic hydrogenation (TCH), thus providing a green and energy efficient alternative.

In this review, we discussed the electrocatalytic valorization of lignin (oxidation and reduction) with particular focus on lignin monomers/dimers, technical lignin, and bio-oil fractions. We also highlighted recent advances in catalyst development and electrode preparation strategies.

Numerous advanced catalysts were developed for the electrocatalytic valorization of lignin, but the key metrics (selectivity, FE, and yield) need significant enhancements. For EO, transition metal catalysts or their alloys (Ni, Co, and Mn) are the best choices for oxidation of lignin or its model compounds, making them cost-effective and scalable. However, further modification is necessary to improve the selectivity, and yield of the targeted product. The oxides of Ru and Ir are highly active but result in overoxidation and are expensive, while Pb-based oxides suffer from surface passivation and have toxicity issues. All current catalysts for lignin depolymerization suffer from product selectivity; further development is needed to produce selective products and improve the efficiency of the electrochemical process. For ECH, noble metals and their alloys (Pt, Rh, Au, and Ru) are widely used due to their high activity toward ring saturation and stability in acidic media. However, high HER occurs especially on Pt and Rh, which hinders the hydrogenation process and results in decreased energy efficiency and FE. To mitigate this, doping with transition metals is a good choice to suppress HER and improve hydrogenation selectivity. In this context, alloy formation and metal–support synergy exhibit significant catalytic activity, providing guidance for designing future catalysts for lignin valorization. Furthermore, computational simulations are necessary for an excellent catalyst design to predict catalytic behavior in these reactions. Above all, there are several challenges that need to be overcome for commercial applications of biorefineries. For lignin valorization, various processes are carried out, such as extraction, separation, and depolymerization of lignin, followed by upgrading *via* electrocatalytic oxidation or reduction. Considerable effort is still needed to perform electrocatalytic valorization at a small scale in a reliable way. The following challenges and research gaps are highlighted for future exploration and advancement to make this process viable for commercial applications:

(1) The utilization of ILs and DESs can enhance lignin dissolution as well as provide a wider potential window than aqueous electrolytes, suppressing the competitive OER and HER.

(2) To gain deeper mechanistic insight and bond cleavage pathways, lignin model compounds with various inter-unit linkages should be systematically studied.

(3) Rational catalyst design is needed to improve reaction rates, selectivity, and faradaic efficiency, and lower operating overpotential by suppressing HER.

(4) The transformation of the electrocatalytic process to a continuous flow process for extracting native lignin from lignocellulosic biomass. This process should be coupled with an electrochemical flow cell for stabilization of monomers, with large electrolyte storage tanks being ideal.

(5) An electrochemical cell with multi-subprocesses (simultaneous oxidation and reduction), such as lignin depolymerization at the anode and its upgrading at the cathode, incorporated in a single operating unit. A similar coupling strategy was employed for glycerol oxidation to glyceraldehyde at the anode alongside guaiacol reduction to cyclohexane at the cathode.[164]

(6) The use of solid polymer electrolyte-based reactors for lignin valorization could operate in a continuous flow mode, replace supporting electrolyte, and save time and effort by extracting products from aqueous media.

(7) Compared to lignin or its model compounds, limited research data are available on bio-oil due to its complex nature with different functional groups. Moreover, low-quality fuel is produced by upgrading bio-oil *via* ECH compared to the traditional hydrodeoxygenation method. Thus, modifying the reactor design to incorporate high temperature and a robust catalyst for both deoxygenation and ECH improves fuel quality.

(8) There is a need for multi-cell electrochemical reactor design for high-throughput screening by mimicking the components of a flow cell electrolyzer (particularly electrode gaps and membrane assembly) on a lab-scale aimed to enable commercial-scale application.

The advancement of electrocatalytic conversion of renewable resources such as biomass, CO_2, and plastic waste will facilitate the transition towards a more sustainable society. These efforts will promote a robust circular bioeconomy based on non-fossil resources, creating new opportunities for sustainable chemical production and climate-neutral technologies.

Author contributions

Majd Al-Naji conceived and designed the study, developed the overall concept of the manuscript, and revised and corrected the final draft. Muhammad Bilal prepared the first draft of the manuscript and carried out subsequent revisions. All other co-authors (Prashanth W. Menezes, Arne Thomas, Reinhard Schomäcker, Matthias Drieß, and Frank Rosowski) contributed by reviewing and critically revising the manuscript prior to submission.

Conflicts of interest

There are no conflicts to declare.

Data availability

This review article does not report any new primary data. All data analyzed or referenced in this work are available in the published literature and have been cited accordingly. No new datasets were generated or analyzed during the preparation of this manuscript.

Acknowledgements

References

1 N. S. Lewis and D. G. Nocera, *Proc. Natl. Acad. Sci. U. S. A.*, 2006, **103**, 15729–15735.

2 Y. Zhu, J. Wang, T. Koketsu, M. Kroschel, J.-M. Chen, S.-Y. Hsu, G. Henkelman, Z. Hu, P. Strasser and J. Ma, *Nat. Commun.*, 2022, **13**, 7754.

3 M. M. Abu-Omar, K. Barta, G. T. Beckham, J. S. Luterbacher, J. Ralph, R. Rinaldi, Y. Román-Leshkov, J. S. M. Samec, B. F. Sels and F. Wang, *Energy Environ. Sci.*, 2021, **14**, 262–292.

4 M. Al-Naji, H. Schlaad and M. Antonietti, *Macromol. Rapid Commun.*, 2021, **42**, 2000485.

5 J. J. Bozell and G. R. Petersen, *Green Chem.*, 2010, **12**, 539.

6 M. Al-Naji, F. Brandi, M. Drieß and F. Rosowski, *Chem. Ing. Tech.*, 2022, **94**, 1611–1627.

7 S. K. Singh, *J. Cleaner Prod.*, 2021, **279**, 123546.

8 R. Biswas, H. Uellendahl and B. K. Ahring, *Bioenergy Res.*, 2015, **8**, 1101–1116.

9 C.-H. Zhou, X. Xia, C.-X. Lin, D.-S. Tong and J. Beltramini, *Chem. Soc. Rev.*, 2011, **40**, 5588.

10 E. Taarning, C. M. Osmundsen, X. Yang, B. Voss, S. I. Andersen and C. H. Christensen, *Energy Environ. Sci.*, 2011, **4**, 793–804.

11 P. Sudarsanam, R. Zhong, S. Van Den Bosch, S. M. Coman, V. I. Parvulescu and B. F. Sels, *Chem. Soc. Rev.*, 2018, **47**, 8349–8402.

12 F. Brandi and M. Al-Naji, *ChemSusChem*, 2022, **15**, e202102525.

13 D. Mohan, C. U. Pittman and P. H. Steele, *Energy Fuels*, 2006, **20**, 848–889.

14 F. Brandi, I. Khalil, M. Antonietti and M. Al-Naji, *ACS Sustainable Chem. Eng.*, 2021, **9**, 927–935.

15 T. Renders, S. Van Den Bosch, S.-F. Koelewijn, W. Schutyser and B. F. Sels, *Energy Environ. Sci.*, 2017, **10**, 1551–1557.

16 D. M. Alonso, J. Q. Bond and J. A. Dumesic, *Green Chem.*, 2010, **12**, 1493.

17 C. A. Smith, F. Brandi, M. Al-Naji and R. Guterman, *RSC Adv.*, 2021, **11**, 15835–15840.

18 M. Al-Naji, M. Popova, Z. Chen, N. Wilde and R. Gläser, *ACS Sustainable Chem. Eng.*, 2020, **8**, 393–402.

19 Z. Sun, B. Fridrich, A. De Santi, S. Elangovan and K. Barta, *Chem. Rev.*, 2018, **118**, 614–678.

20 J. S. Luterbacher, D. Martin Alonso and J. A. Dumesic, *Green Chem.*, 2014, **16**, 4816–4838.

21 J. Zakzeski, P. C. A. Bruijnincx, A. L. Jongerius and B. M. Weckhuysen, *Chem. Rev.*, 2010, **110**, 3552–3599.

22 Y. M. Questell-Santiago, M. V. Galkin, K. Barta and J. S. Luterbacher, *Nat. Rev. Chem.*, 2020, **4**, 311–330.

23 R. Rinaldi, R. Jastrzebski, M. T. Clough, J. Ralph, M. Kennema, P. C. A. Bruijnincx and B. M. Weckhuysen, *Angew. Chem., Int. Ed.*, 2016, **55**, 8164–8215.

24 S. Stiefel, J. Lölsberg, L. Kipshagen, R. Möller-Gulland and M. Wessling, *Electrochem. Commun.*, 2015, **61**, 49–52.

25 W. Schutyser, T. Renders, S. Van Den Bosch, S.-F. Koelewijn, G. T. Beckham and B. F. Sels, *Chem. Soc. Rev.*, 2018, **47**, 852–908.

26 D. L. Klass, *Biomass for Renewable Energy, Fuels, and Chemicals*, Academic Press, San Diego, 1998.

27 I. Romanenko, F. Kurz, R. Baumgarten, I. Jevtovikj, J.-P. Lindner, A. Kundu, A. Kindler and S. A. Schunk, *Catalysts*, 2022, **12**, 158.

28 W. Guan, C.-W. Tsang, C. S. K. Lin, C. Len, H. Hu and C. Liang, *Bioresour. Technol.*, 2020, **298**, 122432.

29 R. Sun, *Cereal Straw as a Resource for Sustainable Biomaterials and Biofuels: Chemistry, Extractives, Lignins, Hemicelluloses and Cellulose*, Elsevier, Amsterdam, 2010.

30 H. Lange, S. Decina and C. Crestini, *Eur. Polym. J.*, 2013, **49**, 1151–1173.

31 B. Nanayakkara, M. Manley-Harris, I. D. Suckling and L. A. Donaldson, *Holzforschung*, 2009, **63**, 431–439.

32 Md. R. Islam, *J. Microbiol. Biotechnol.*, 2009, **19**(10), 1213–1222.

33 S. Van Den Bosch, W. Schutyser, R. Vanholme, T. Driessen, S.-F. Koelewijn, T. Renders, B. De Meester, W. J. J. Huijgen, W. Dehaen, C. M. Courtin, B. Lagrain, W. Boerjan and B. F. Sels, *Energy Environ. Sci.*, 2015, **8**, 1748–1763.

34 J. C. Del Río, J. Rencoret, P. Prinsen, Á. T. Martínez, J. Ralph and A. Gutiérrez, *J. Agric. Food Chem.*, 2012, **60**, 5922–5935.

35 D. S. Bajwa, D. Pourhashem, A. H. Ullah and S. G. Bajwa, *Ind. Crops Prod.*, 2019, **139**, 111526.

36 C. Li, X. Zhao, A. Wang, G. W. Huber and T. Zhang, *Chem. Rev.*, 2015, **115**, 11559–11624.

37 Y. Cao, M. He, S. Dutta, G. Luo, S. Zhang and D. C. W. Tsang, *Renewable Sustainable Energy Rev.*, 2021, **152**, 111722.

38 S. K. Singh, *Bioresour. Technol. Rep.*, 2022, **17**, 100958.

39 *Biorefinery: from Biomass to Chemicals and Fuels*, ed. M. Aresta, de Gruyter, Berlin, 2012.

40 A. Ekielski and P. K. Mishra, *Int. J. Mol. Sci.*, 2020, **22**, 63.

41 X. Shen, C. Zhang, B. Han and F. Wang, *Chem. Soc. Rev.*, 2022, **51**, 1608–1628.

42 K. Routray, K. J. Barnett and G. W. Huber, *Energy Technol.*, 2017, **5**, 80–93.

43 Y. P. Wijaya, K. J. Smith, C. S. Kim and E. L. Gyenge, *Green Chem.*, 2020, **22**, 7233–7264.

44 Y. Liao, S.-F. Koelewijn, G. Van Den Bossche, J. Van Aelst, S. Van Den Bosch, T. Renders, K. Navare, T. Nicolaï, K. Van Aelst, M. Maesen, H. Matsushima, J. M. Thevelein, K. Van Acker, B. Lagrain, D. Verboekend and B. F. Sels, *Science*, 2020, **367**, 1385–1390.

45 M. G. A. Da Cruz, B. V. M. Rodrigues, A. Ristic, S. Budnyk, S. Das and A. Slabon, *Green Chem. Lett. Rev.*, 2022, **15**, 153–161.

46 M. Garedew, F. Lin, B. Song, T. M. DeWinter, J. E. Jackson, C. M. Saffron, C. H. Lam and P. T. Anastas, *ChemSusChem*, 2020, **13**, 4214–4237.

47 B. H. Nguyen, R. J. Perkins, J. A. Smith and K. D. Moeller, *J. Org. Chem.*, 2015, **80**, 11953–11962.

48 W. Shen, X. Chen, J. Qiu, J. A. Hayward, S. Sayeef, P. Osman, K. Meng and Z. Y. Dong, *Renewable Sustainable Energy Rev.*, 2020, **133**, 110301.

49 T. Möller, M. Filippi, S. Brückner, W. Ju and P. Strasser, *Nat. Commun.*, 2023, **14**, 5680.

50 P. Hauke, T. Merzdorf, M. Klingenhof and P. Strasser, *Nat. Commun.*, 2023, **14**, 4708.

51 J. Xu, J. Meng, Y. Hu, Y. Liu, Y. Lou, W. Bai, S. Dou, H. Yu and S. Wang, *Research*, 2023, **6**, 0288.

52 N. Casado, M. Hilder, C. Pozo-Gonzalo, M. Forsyth and D. Mecerreyes, *ChemSusChem*, 2017, **10**, 1783–1791.

53 A. L. Rauen, F. Weinelt and S. R. Waldvogel, *Green Chem.*, 2020, **22**, 5956–5960.

54 A. Das, A. Rahimi, A. Ulbrich, M. Alherech, A. H. Motagamwala, A. Bhalla, L. Da Costa Sousa, V. Balan, J. A. Dumesic, E. L. Hegg, B. E. Dale, J. Ralph, J. J. Coon and S. S. Stahl, *ACS Sustainable Chem. Eng.*, 2018, **6**, 3367–3374.

55 J. Luo and T. L. Liu, *J. Bioresour. Bioprod.*, 2023, **8**, 1–14.

56 T. De Saegher, J. Lauwaert, J. Vercammen, K. M. Van Geem, J. De Clercq and A. Verberckmoes, *ChemistryOpen*, 2021, **10**, 740–747.

57 Z. Ebrahimpourboura, M. Mosalpuri, C. Yang, A. Ponukumati, C. Stephenson, M. Foston and M. M. Wright, *Green Chem.*, 2024, **26**, 11303–11315.

58 X. Du, H. Zhang, K. P. Sullivan, P. Gogoi and Y. Deng, *ChemSusChem*, 2020, **13**, 4318–4343.

59 A. Tribot, G. Amer, M. Abdou Alio, H. De Baynast, C. Delattre, A. Pons, J.-D. Mathias, J.-M. Callois, C. Vial, P. Michaud and C.-G. Dussap, *Eur. Polym. J.*, 2019, **112**, 228–240.

60 R. Hu, Y. Zhao, C. Tang, Y. Shi, G. Luo, J. Fan, J. H. Clark and S. Zhang, *Engineering*, 2023, **27**, 178–198.

61 Q. Zhu, M. Garedew, B. Song, Y. Li and J. C. Lam, in *Lignin Chemistry*, ed Y. Liao and B. F. Sels, Wiley, 1st edn, 2024, pp. 295–326.

62 X. Liu, Y. Wang and H. Duan, *Precis. Chem.*, 2024, **2**, 428–446.

63 X. Du, W. Liu, Z. Zhang, A. Mulyadi, A. Brittain, J. Gong and Y. Deng, *ChemSusChem*, 2017, **10**, 847–854.

64 H. Zhu, Y. Chen, T. Qin, L. Wang, Y. Tang, Y. Sun and P. Wan, *RSC Adv.*, 2014, **4**, 6232.

65 E. Reichert, R. Wintringer, D. A. Volmer and R. Hempelmann, *Phys. Chem. Chem. Phys.*, 2012, **14**, 5214.

66 P. Cai, H. Fan, S. Cao, J. Qi, S. Zhang and G. Li, *Electrochim. Acta*, 2018, **264**, 128–139.

67 Z. Lu, B. Tu and F. Chen, *J. Wood Chem. Technol.*, 2003, **23**, 261–277.

68 D. Di Marino, D. Stöckmann, S. Kriescher, S. Stiefel and M. Wessling, *Green Chem.*, 2016, **18**, 6021–6028.

69 T. Shiraishi, T. Takano, H. Kamitakahara and F. Nakatsubo, *Holzforschung*, 2012, **66**(3), 311–315.

70 L. Yang, W. Liu, Z. Zhang, X. Du, J. Gong, L. Dong and Y. Deng, *Electrochim. Acta*, 2017, **246**, 1163–1173.

71 A. Rahimi, A. Azarpira, H. Kim, J. Ralph and S. S. Stahl, *J. Am. Chem. Soc.*, 2013, **135**, 6415–6418.

72 C. Zhang, H. Li, J. Lu, X. Zhang, K. E. MacArthur, M. Heggen and F. Wang, *ACS Catal.*, 2017, **7**, 3419–3429.

73 C. S. Lancefield, O. S. Ojo, F. Tran and N. J. Westwood, *Angew. Chem.*, 2015, **127**, 260–264.

74 S. Ljunggren and A. Olsson, *Holzforschung*, 1984, **38**, 91–99.

75 E. Baciocchi, M. Bietti and O. Lanzalunga, *Acc. Chem. Res.*, 2000, **33**, 243–251.

76 S. B. Lalvani and P. Rajagopal, *Holzforschung*, 1993, **47**, 283–286.

77 M. NaderiNasrabadi, F. Bateni, Z. Chen, P. B. Harrington and J. A. Staser, *J. Electrochem. Soc.*, 2019, **166**, E317–E322.

78 F. Bateni, M. NaderiNasrabadi, R. Ghahremani and J. A. Staser, *J. Electrochem. Soc.*, 2019, **166**, F1037–F1046.

79 C. Lan, H. Fan, Y. Shang, D. Shen and G. Li, *Sustainable Energy Fuels*, 2020, **4**, 1828–1836.

80 R. Tolba, M. Tian, J. Wen, Z.-H. Jiang and A. Chen, *J. Electroanal. Chem.*, 2010, **649**, 9–15.

81 A. Bailey and H. M. Brooks, *J. Am. Chem. Soc.*, 1946, **68**, 445–446.

82 X. Hao, Y. Quansheng, S. Dan, Y. Honghui, L. Jidong, F. Jiangtao and Y. Wei, *J. Hazard. Mater.*, 2015, **286**, 509–516.

83 D. Rauber, T. K. F. Dier, D. A. Volmer and R. Hempelmann, *Z. Phys. Chem.*, 2018, **232**, 189–208.

84 H. Su, Y. Ye, K.-J. Lee, J. Zeng and E. J. Crumlin, *J. Phys. D: Appl. Phys.*, 2021, **54**, 374001.

85 O. Movil, M. Garlock and J. A. Staser, *Int. J. Hydrogen Energy*, 2015, **40**, 4519–4530.

86 A. J. Bard and L. R. Faulkner, *Electrochemical Methods*, Wiley, 2nd edn, 2012.

87 O. Movil-Cabrera, A. Rodriguez-Silva, C. Arroyo-Torres and J. A. Staser, *Biomass Bioenergy*, 2016, **88**, 89–96.

88 Y. Sannami, H. Kamitakahara and T. Takano, *Holzforschung*, 2017, **71**, 109–117.

89 M. Rafiee, M. Alherech, S. D. Karlen and S. S. Stahl, *J. Am. Chem. Soc.*, 2019, **141**, 15266–15276.

90 W.-J. Gao, C. M. Lam, B.-G. Sun, R. D. Little and C.-C. Zeng, *Tetrahedron*, 2017, **73**, 2447–2454.

91 G. Liu, Q. Wang, D. Yan, Y. Zhang, C. Wang, S. Liang, L. Jiang and H. He, *Green Chem.*, 2021, **23**, 1665–1677.

92 H. Zhu, L. Wang, Y. Chen, G. Li, H. Li, Y. Tang and P. Wan, *RSC Adv.*, 2014, **4**, 29917.

93 L. Wang, S. Liu, H. Jiang, Y. Chen, L. Wang, G. Duan, Y. Sun, Y. Chen and P. Wan, *J. Electrochem. Soc.*, 2018, **165**, H705–H710.

94 L. Ma, H. Zhou, X. Kong, Z. Li and H. Duan, *ACS Sustainable Chem. Eng.*, 2021, **9**, 1932–1940.

95 A. Caravaca, W. E. Garcia-Lorefice, S. Gil, A. De Lucas-Consuegra and P. Vernoux, *Electrochem. Commun.*, 2019, **100**, 43–47.

96 M. Zirbes, D. Schmitt, N. Beiser, D. Pitton, T. Hoffmann and S. R. Waldvogel, *ChemElectroChem*, 2019, **6**, 155–161.

97 Q. Li, J. Jiang, G. Li, W. Zhao, X. Zhao and T. Mu, *Sci. China:Chem.*, 2016, **59**, 571–577.

98 W. Ma, G. Liu, Q. Wang, J. Liu, X. Yuan, J. Xin, S. Wang and H. He, *J. Mol. Liq.*, 2022, **367**, 120407.

99 T. K. F. Dier, D. Rauber, D. Durneata, R. Hempelmann and D. A. Volmer, *Sci. Rep.*, 2017, **7**, 5041.

100 S. Stiefel, A. Schmitz, J. Peters, D. Di Marino and M. Wessling, *Green Chem.*, 2016, **18**, 4999–5007.

101 D. Di Marino, V. Aniko, A. Stocco, S. Kriescher and M. Wessling, *Green Chem.*, 2017, **19**, 4778–4784.

102 B. Zhang, J. Zhang and Z. Zhong, *ACS Appl. Energy Mater.*, 2018, **1**, 6758–6763.

103 S. Xiu and A. Shahbazi, *Renewable Sustainable Energy Rev.*, 2012, **16**, 4406–4414.

104 M. Bilal and M. Al-Naji, *Discov. Catal.*, 2025, **2**, 10.

105 M. Saidi, F. Samimi, D. Karimipourfard, T. Nimmanwudipong, B. C. Gates and M. R. Rahimpour, *Energy Environ. Sci.*, 2014, **7**, 103–129.

106 H. P. Godard, J. L. McCarthy and H. Hibbert, *J. Am. Chem. Soc.*, 1940, **62**, 988.

107 T. Renders, G. Van Den Bossche, T. Vangeel, K. Van Aelst and B. Sels, *Curr. Opin. Biotechnol.*, 2019, **56**, 193–201.

108 T. Renders, E. Cooreman, S. Van Den Bosch, W. Schutyser, S.-F. Koelewijn, T. Vangeel, A. Deneyer, G. Van Den Bossche, C. M. Courtin and B. F. Sels, *Green Chem.*, 2018, **20**, 4607–4619.

109 W. Schutyser, S. Van Den Bosch, T. Renders, T. De Boe, S.-F. Koelewijn, A. Dewaele, T. Ennaert, O. Verkinderen, B. Goderis, C. M. Courtin and B. F. Sels, *Green Chem.*, 2015, **17**, 5035–5045.

110 K. Van Aelst, E. Van Sinay, T. Vangeel, E. Cooreman, G. Van Den Bossche, T. Renders, J. Van Aelst, S. Van Den Bosch and B. F. Sels, *Chem. Sci.*, 2020, **11**, 11498–11508.

111 G. Kreysa, K. Ota and R. F. Savinell, *Encyclopedia of Applied Electrochemistry*, Springer, New York, 2014.

112 R. I. Pacut and E. Kariv-Miller, *J. Org. Chem.*, 1986, **51**, 3468–3470.

113 Z. Fang, M. G. Flynn, J. E. Jackson and E. L. Hegg, *Green Chem.*, 2021, **23**, 412–421.

114 Y. Song, S. H. Chia, U. Sanyal, O. Y. Gutiérrez and J. A. Lercher, *J. Catal.*, 2016, **344**, 263–272.

115 Z. Li, M. Garedew, C. H. Lam, J. E. Jackson, D. J. Miller and C. M. Saffron, *Green Chem.*, 2012, **14**, 2540.

116 Y. Du, X. Chen and C. Liang, *Mol. Catal.*, 2023, **535**, 112831.

117 M. Garedew, D. Young-Farhat, S. Bhatia, P. Hao, J. E. Jackson and C. M. Saffron, *Sustainable Energy Fuels*, 2020, **4**, 1340–1350.

118 K. Amouzegar and O. Savadogo, *Electrochim. Acta*, 1994, **39**, 557–559.

119 Y. P. Wijaya, T. Grossmann-Neuhaeusler, R. D. Dhewangga Putra, K. J. Smith, C. S. Kim and E. L. Gyenge, *ChemSusChem*, 2020, **13**, 629–639.

120 W. Liu, W. You, Y. Gong and Y. Deng, *Energy Environ. Sci.*, 2020, **13**, 917–927.

121 P. Zhou, S. Guo, L. Li, T. Ueda, Y. Nishiwaki, L. Huang, Z. Zhang and J. Zhang, *Angew. Chem., Int. Ed.*, 2023, **62**, e202214881.

122 X. Chen, X. Liu, X. Yang, Y. Qi, Y. Wang, J. Sun, F. Zhao and L. Zhang, *Adv. Sustainable Syst.*, 2025, **9**, e00422.

123 M. Wang, T. Peng, C. Yang, B. Liang, H. Chen, M. Kumar, Y. Zhang and W. Zhao, *Green Chem.*, 2022, **24**, 142–146.

124 C. H. Lam, C. B. Lowe, Z. Li, K. N. Longe, J. T. Rayburn, M. A. Caldwell, C. E. Houdek, J. B. Maguire, C. M. Saffron, D. J. Miller and J. E. Jackson, *Green Chem.*, 2015, **17**, 601–609.

125 Y. Zhou, Y. Gao, X. Zhong, W. Jiang, Y. Liang, P. Niu, M. Li, G. Zhuang, X. Li and J. Wang, *Adv. Funct. Mater.*, 2019, **29**, 1807651.

126 T. Peng, W. Zhang, B. Liang, G. Lian, Y. Zhang and W. Zhao, *Nat. Commun.*, 2023, **14**, 7229.

127 T. Peng, T. Zhuang, Y. Yan, J. Qian, G. R. Dick, J. Behaghel De Bueren, S.-F. Hung, Y. Zhang, Z. Wang, J. Wicks, F. P. Garcia De Arquer, J. Abed, N. Wang, A. Sedighian Rasouli, G. Lee, M. Wang, D. He, Z. Wang, Z. Liang, L. Song, X. Wang, B. Chen, A. Ozden, Y. Lum, W. R. Leow, M. Luo, D. M. Meira, A. H. Ip, J. S. Luterbacher, W. Zhao and E. H. Sargent, *J. Am. Chem. Soc.*, 2021, **143**, 17226–17235.

128 M. Yang, L. Li, J. Shi, H. Xia and J. Xu, *Biomass Convers. Biorefin.*, 2025, **15**, 9047–9057.

129 J. A. Lopez-Ruiz, U. Sanyal, J. Egbert, O. Y. Gutiérrez and J. Holladay, *ACS Sustainable Chem. Eng.*, 2018, **6**, 16073–16085.

130 Y. Song, O. Y. Gutiérrez, J. Herranz and J. A. Lercher, *Appl. Catal., B*, 2016, **182**, 236–246.

131 N. Singh, U. Sanyal, G. Ruehl, K. A. Stoerzinger, O. Y. Gutiérrez, D. M. Camaioni, J. L. Fulton, J. A. Lercher and C. T. Campbell, *J. Catal.*, 2020, **382**, 372–384.

132 H. Liu, T. Jiang, B. Han, S. Liang and Y. Zhou, *Science*, 2009, **326**, 1250–1252.

133 B. Zhao, Q. Guo and Y. Fu, *Electrochemistry*, 2014, **82**, 954–959.

134 N. Singh, Y. Song, O. Y. Gutiérrez, D. M. Camaioni, C. T. Campbell and J. A. Lercher, *ACS Catal.*, 2016, **6**, 7466–7470.

135 Y. P. Wijaya, K. J. Smith, C. S. Kim and E. L. Gyenge, *J. Appl. Electrochem.*, 2021, **51**, 51–63.

136 L. Zhou, X. Zhu, H. Su, H. Lin, Y. Lyu, X. Zhao, C. Chen, N. Zhang, C. Xie, Y. Li, Y. Lu, J. Zheng, B. Johannessen, S. P. Jiang, Q. Liu, Y. Li, Y. Zou and S. Wang, *Sci. China:Chem.*, 2021, **64**, 1586–1595.

137 S. Tong, X. Gao, H. Zhou, Q. Shi, Y. Wu and W. Chen, *Inorg. Chem.*, 2023, **62**, 19123–19134.

138 Y. P. Wijaya, R. D. D. Putra, K. J. Smith, C. S. Kim and E. L. Gyenge, *ACS Sustainable Chem. Eng.*, 2021, **9**, 13164–13175.

139 S. Han, X. Zhang, R. Wang, K. Wang, J. Jiang and J. Xu, *Chem. Eng. J.*, 2023, **452**, 139299.

140 Y. Song, U. Sanyal, D. Pangotra, J. D. Holladay, D. M. Camaioni, O. Y. Gutiérrez and J. A. Lercher, *J. Catal.*, 2018, **359**, 68–75.

141 J. A. Lopez-Ruiz, E. Andrews, S. A. Akhade, M.-S. Lee, K. Koh, U. Sanyal, S. F. Yuk, A. J. Karkamkar, M. A. Derewinski, J. Holladay, V.-A. Glezakou, R. Rousseau, O. Y. Gutiérrez and J. D. Holladay, *ACS Catal.*, 2019, **9**, 9964–9972.

142 Y. Wu, Z. Guo, C. Sun, X. Ren and Q. Li, *Fuel Process. Technol.*, 2022, **237**, 107436.

143 G. Cheng, Z. Zhai, J. Sun, Y. Ran, W. Yang, F. Tan and Z. Zhang, *Chem. Eng. J.*, 2023, **474**, 145631.

144 Q. Yang, B. Ge, P. Yuan, S. Luo, H. Zhang, Z. Zhao, J. Zhang, S. Wang, X. Bao and X. Yao, *Adv. Funct. Mater.*, 2023, **33**, 2214588.

145 B. Mahdavi, A. Lafrance, A. Martel, J. Lessard, H. MéNard and L. Brossard, *J. Appl. Electrochem.*, 1997, **27**, 605–611.

146 N. Yao, P. Li, Z. Zhou, Y. Zhao, G. Cheng, S. Chen and W. Luo, *Adv. Energy Mater.*, 2019, **9**, 1902449.

147 M. G. A. Da Cruz, R. Gueret, J. Chen, J. Piątek, B. Beele, M. H. Sipponen, M. Frauscher, S. Budnyk, B. V. M. Rodrigues and A. Slabon, *ChemSusChem*, 2022, **15**, e202200718.

148 L. M. Lindenbeck, V. C. Barra, S. Dahlhaus, S. Brand, L. M. Wende, B. B. Beele, N. H. Schebb, B. V. M. Rodrigues and A. Slabon, *ChemSusChem*, 2024, **17**, e202301617.

149 L. Lindenbeck, S. Brand, F. Stallmann, V. Barra, M. Frauscher, B. B. Beele, A. Slabon and B. V. M. Rodrigues, *Polymers*, 2024, **16**, 3325.

150 Z. Li, S. Kelkar, L. Raycraft, M. Garedew, J. E. Jackson, D. J. Miller and C. M. Saffron, *Green Chem.*, 2014, **16**, 844–852.

151 W. Deng, K. Xu, Z. Xiong, W. Chaiwat, X. Wang, S. Su, S. Hu, J. Qiu, Y. Wang and J. Xiang, *Energy Fuels*, 2019, **33**, 11292–11301.

152 D. S. Santana, G. O. Melo, M. V. F. Lima, J. R. R. Daniel, M. C. C. Areias and M. Navarro, *J. Electroanal. Chem.*, 2004, **569**, 71–78.

153 D. Schmitt, C. Regenbrecht, M. Hartmer, F. Stecker and S. R. Waldvogel, *Beilstein J. Org. Chem.*, 2015, **11**, 473–480.

154 J. Klein and S. R. Waldvogel, *ChemSusChem*, 2023, **16**, e202202300.

155 M. Zirbes, T. Graßl, R. Neuber and S. R. Waldvogel, *Angew. Chem., Int. Ed.*, 2023, **62**, e202219217.

156 M. Garedew, D. Young-Farhat, J. E. Jackson and C. M. Saffron, *ACS Sustainable Chem. Eng.*, 2019, **7**, 8375–8386.

157 Q. Zhou, R. Chen, Y. Chen, Y. Sun, J. Yuan, J. Xu, X. Liao, B. Shi and X. Xiao, *Ind. Crops Prod.*, 2025, **229**, 120977.

158 Z. Gu, Z. Zhang, N. Ni, C. Hu and J. Qu, *Environ. Sci. Technol.*, 2022, **56**, 4356–4366.

159 T. Peng, T. Zhuang, Y. Yan, J. Qian, G. Dick, J. B. De Bueren, S.-F. Hung, Z. Wang, J. Wicks, F. P. G. De Arquer, J. Abed, N. Wang, A. Rasouli, G. Lee, M. Wang, D. He, Z. Wang, Z. Liang, L. Song, X. Wang, B. Chen, A. Ozden, Y. Lum, W. R. Leow, M. Luo, D. Meira, A. Ip, J. Luterbacher, W. Zhao and E. Sargent, in *Review*, 2021, DOI: 10.21203/rs.3.rs-131880/v1.

160 A. Cyr, F. Chiltz, P. Jeanson, A. Martel, L. Brossard, J. Lessard and H. Ménard, *Can. J. Chem.*, 2000, **78**, 307–315.

161 C. Yang, H. Chen, T. Peng, B. Liang, Y. Zhang and W. Zhao, *Chin. J. Catal.*, 2021, **42**, 1831–1842.

162 D. Pletcher, *J. Electroanal. Chem.*, 2001, **502**, 204.

163 E. Andrews, J. A. Lopez-Ruiz, J. D. Egbert, K. Koh, U. Sanyal, M. Song, D. Li, A. J. Karkamkar, M. A. Derewinski, J. Holladay, O. Y. Gutiérrez and J. D. Holladay, *ACS Sustainable Chem. Eng.*, 2020, **8**, 4407–4418.

164 F. A. Setiawan, I. S. Y. Louise, K. J. Smith, C. S. Kim and E. L. Gyenge, *ACS Sustainable Chem. Eng.*, 2025, **13**, 7803–7811.